

A method to derive material-specific model descriptions of spin degrees of freedom coupled to a fermionic bath for materials displaying prevalent spin physics

Benedikt M. Schoenauer,* Nicklas Enenkel, Florian G. Eich, Vladimir V.

Rybkin, Michael Marthaler, Sebastian Zanker, and Peter Schmitteckert†

HQS Quantum Simulations GmbH, Rintheimer Straße 23, 76131 Karlsruhe, Germany

(Dated: September 9, 2025)

Magnetism and spin physics are true quantum mechanical effects and their description usually requires multi reference methods and is often hidden in the standard description of molecules in quantum chemistry. In this work we present a twofold approach to the description of spin physics in molecules and solids. First, we present a method that identifies the single-particle basis in which a given subset of the orbitals is equivalent to spin degrees of freedom for models and materials which feature significant spin physics at low energies. We introduce a metric for the spin-like character of a basis orbital, of which the optimization yields the basis containing the optimum spin-like basis orbitals. Second, we demonstrate an extended Schrieffer-Wolff transformation method to derive the effective Hamiltonian acting on the subspace of the Hilbert space in which the charge degree of freedom of electron densities in the spin-like orbitals is integrated out. The method then yields an effective Hamiltonian describing spins coupled to a fermionic environment. This extended Schrieffer-Wolff transformation is applicable to a wide range of Hamiltonians and has been utilized in this work for model Hamiltonians as well as the Hamiltonian describing the active orbital space of molecular chromium bromide. This is achieved by reformulating the highly non-linear Schrieffer-Wolff equations into a linear set of equations corresponding to an operator basis.

I. INTRODUCTION

The theoretical study of the physics of many-body quantum systems has remained notoriously difficult on conventional computers not least due to the intractable exponential growth of the corresponding Hilbert spaces. This holds true already for simple model Hamiltonians, but becomes even more problematic for the study of real materials due to the vast number of degrees of freedom and interactions. To investigate certain aspects of these materials it is therefore imperative to either utilize significant approximations or to obtain a much more concise Hamiltonian focused on accurately describing this aspect. In this article, we concentrate on the description of the spin physics of actual materials. The spin physics is relevant for the understanding of the material's magnetic properties [1] as well as their experimental identification with spin resonance spectroscopy techniques [2, 3]. The quantum simulation of spin system Hamiltonians is also perfectly suited as an application of quantum computing in general [4] and analogue quantum computing in particular[5].

We present a method for the derivation of the effective Hamiltonian description for the relevant spin degrees of freedom of an actual material embedded in an environment of fermions. The first part of the method entails the identification of potential relevant orbital spin degrees of freedom. We propose a new metric for the classification of orbital spin degrees of freedom and present a systematic way to determine the orbital basis that contains

the best realizations of these spins, see also [6]. Given the presence of relevant spins, we proceed with the second part of the method, a Schrieffer-Wolff transformation procedure [7, 8] aimed at decoupling the subspace of the Hilbert space containing these spin degrees of freedom from the remaining high-energy subspaces containing the charge degrees of freedom. Many different Schrieffer-Wolff and related unitary transformation schemes have been proposed, comprising perturbative [7, 9, 10], variational [11], and continuous [12–14] variants. So far, the application of these methods has been limited to concise model Hamiltonians. We present an extended version of the perturbative single step Schrieffer-Wolff transformation that can be applied to generic Hamiltonian descriptions of materials, given the presence of relevant low-energy spin physics in the material. By restricting ourselves to spin-like orbitals that have by definition no or only small charge fluctuations we ensure that a perturbative treatment of the charge fluctuations is justified. This is also a main difference to canonical transformation approaches [15] where one tries to achieve a canonical diagonalization. We restrict our canonical transformation to a perturbative regime where the application does not create large higher order terms.

We demonstrate the accuracy of the effective spin-bath model Hamiltonians, where the spin-like orbitals are treated as spins coupled to a fermionic bath, resulting from our Schrieffer-Wolff transformation for the description of the low-energy physics both for simple model Hamiltonians with established results [7, 16] as well as actual materials. We further discuss the extent to which the quality of the effective model Hamiltonian for the spins coupled to the fermionic environment derived with the proposed method can be anticipated.

We would like to point out that we do start with an ap-

* benedikt.schoenauer@quantumsimulations.de

† peter.schmitteckert@quantumsimulations.de

proximate multi reference calculation to determine a suitable single particle basis. However, the Schrieffer-Wolff expansion, as explained below, starts from the full quantum chemical description only using the adapted basis set from the multi reference calculation. At first glance this may appear as a waste of resources. However, as shown below, already starting in a suitable single particle basis leads to a reasonably good spin-bath model, which then improved by the Schrieffer Wolff transformation. This approach is in strong contrast to a traditional setup, where one tries to extract either an effective Hubbard model using DFT+U [17, 18], DFT+DMFT [19–21] or constrained RPA [22–26] in the framework of maximally localized Wannier functions [27–29], which is can then be transformed into a spin-math model. Or alternatively using DFT based approaches using the magnetic force theorem [30, 31]. In these approaches various approximation are staggered. In our work we only rely on the Schrieffer-Wolff transformation.

II. METHODOLOGY

In Section II A we define the notion of spin-like orbitals and in Section II B we propose the local parity as a metric for the spin-like character of orbitals. In Section II C we present our parity optimization procedure as a way to determine spin-like orbitals, as well as a way to gauge the presence of relevant low energy spin physics in the system. We discuss the basic concept of the Schrieffer-Wolff transformation in Section II D. We provide our proposed extended Schrieffer-Wolff transformation method in detail in Sections II E and II F. In Section II G we show how the described methods are combined into our workflow for deriving effective model Hamiltonians of spins in a fermionic environment for materials with relevant low-energy spin physics.

A. Spin-like orbitals

We consider an orbital ϕ_i as being spin-like only if the electron density n_i contained in it is strictly equal to one. This requires that the average electron density in the orbitals ϕ_i satisfies $\langle n_i \rangle = 1$. It furthermore requires that the fluctuations around this average electron density satisfy $\delta n_i \rightarrow 0$. Negligible fluctuations around the average electron density imply that electron density of the orbital does not affect the low-energy dynamics of the system and vice versa. Just an average electron density $\langle n_i \rangle = 1$ places no restrictions on the orientation and dynamics of the electron spin in the orbital ϕ_i . When both requirements are simultaneously met by the states in the low-energy Hilbert space, the dynamics of the electron density in the orbital ϕ_i , often referred to as the charge degree of freedom, becomes superfluous to the description of the dynamics of the system. The electron density in the orbital ϕ_i consequently couples to the re-

mainder of the system exclusively via its spin degree of freedom. It is then sufficient to represent the degrees of freedom of the electron density contained in the orbital ϕ_i as a pure spin degree of freedom and to employ the associated spin operator algebra. The local Hilbert space \mathcal{H}_i of a spin degree of freedom is half the size of the local Hilbert space of a fermionic orbital and is furthermore naturally represented on a Qubit. We therefore aim to determine each spin-like basis orbital or linear combinations thereof meeting both stated requirements, so that they can be represented as spins.

B. Local parity

We propose the ground state local parity P_i as a measure for the spin-like character of an orbital ϕ_i . The operator representation of the local parity reads

$$P_i = (-1)^{n_{i\uparrow} + n_{i\downarrow}}, \quad (1)$$

where $n_{i\uparrow} = c_{i\uparrow}^\dagger c_{i\uparrow}$ denotes the electron density in ϕ_i with electron spin quantum number $s_i^z = +1/2$ and $n_{i\downarrow} = c_{i\downarrow}^\dagger c_{i\downarrow}$ the electron density with quantum number $s_i^z = -1/2$ respectively, where we are using units with $\hbar = 1$. The local Hilbert space \mathcal{H}_i of the orbital ϕ_i is spanned by the states,

$$\{|0\rangle, |\uparrow\rangle, |\downarrow\rangle, |\uparrow\downarrow\rangle\}, \quad (2)$$

and the action of the local parity operator on these states reads

$$\begin{aligned} P_i |0\rangle &= +1 |0\rangle \\ P_i |\downarrow\rangle &= -1 |\downarrow\rangle \\ P_i |\uparrow\rangle &= -1 |\uparrow\rangle \\ P_i |\uparrow\downarrow\rangle &= +1 |\uparrow\downarrow\rangle. \end{aligned} \quad (3)$$

For states where the orbital contains a single electron the local parity operator P_i returns the eigenvalue $p_i = -1$. For the remaining two basis states P_i returns the eigenvalue $p_i = +1$. Any state $|\psi\rangle$ in the local Hilbert space \mathcal{H}_i that contains contributions from non singly occupied basis states hence satisfies

$$P_i |\psi\rangle = (-1 + \alpha) |\psi\rangle, \quad (4)$$

with $2 \geq \alpha > 0$, because the resulting fluctuations in the electron density $\delta n_i \neq 0$ manifest themselves in strictly positive contributions to the local parity. An alternative and more useful operator representation of the local parity reads

$$\begin{aligned} P_i &= \left(1 - 2c_{i\uparrow}^\dagger c_{i\uparrow}\right) \left(1 - 2c_{i\downarrow}^\dagger c_{i\downarrow}\right) \\ &= 1 - 2 \left(c_{i\uparrow}^\dagger c_{i\uparrow} + c_{i\downarrow}^\dagger c_{i\downarrow}\right) + 4 c_{i\uparrow}^\dagger c_{i\downarrow}^\dagger c_{i\downarrow} c_{i\uparrow}, \end{aligned} \quad (5)$$

and its corresponding expectation value with respect to the many-body state $|n\rangle$ can be expressed as

$$\langle n | P_i | n \rangle = 1 - 2\rho_{ii}^{(1)} + 4\rho_{iiii}^{(2)}, \quad (6)$$

where

$$\rho_{qp}^{(1)} = \sum_{\sigma} \langle n | c_{q\sigma}^{\dagger} c_{p\sigma} | n \rangle, \quad (7)$$

denotes the one-electron reduced density matrix (1-RDM) and

$$\rho_{qprs}^{(2)} = \langle n | c_{q\uparrow}^{\dagger} c_{p\downarrow}^{\dagger} c_{r\downarrow} c_{s\uparrow} | n \rangle, \quad (8)$$

denotes the two-electron reduced density matrix (2-RDM) respectively. If we choose $|n\rangle = |\psi_0\rangle$, with $|\psi_0\rangle$ a good approximation of the ground state of the system, we can identify orbitals ϕ_i for which $\langle P_i \rangle_0 = \langle \psi_0 | P_i | \psi_0 \rangle = -1 + \varepsilon$, with $\varepsilon \rightarrow 0$, as spin-like orbitals of the system. In general, the spin-like orbitals of the system do not coincide with the basis orbitals typically used in standard basis sets of quantum chemistry codes. We therefore require a method to determine the set $\{\phi_i\}$ of orthonormal linear combinations of basis orbitals, for which the local parities most closely approach $\{p_i\} = -1$.

C. Local parity optimization of the orbital basis

We propose an iterative procedure to determine the particular orbital basis in which the local parities are extremal. For this we attempt a sequence of unitary pairwise rotations of the orbital fermionic operators given by

$$\begin{aligned} c_{q\sigma} &= \cos \theta c_{i\sigma} + \sin \theta c_{j\sigma}, \\ c_{p\sigma} &= -\sin \theta c_{i\sigma} + \cos \theta c_{j\sigma}, \end{aligned} \quad (9)$$

with the same rotation being performed for the Hermitian conjugates of the operators. From the reduced density matrices $\rho^{(1)}$ and $\rho^{(2)}$ we can compute the local parity of an orbital ϕ_q , which results from the linear combination of orbitals ϕ_i and ϕ_j , as $\langle P_q \rangle_0(\theta)$. The local parity $\langle P_q \rangle_0(\theta)$ is an analytic, 2π -periodic function of the rotation angle θ . We find the extremal points θ_n of the function $\langle P_q \rangle_0(\theta)$ in the domain $\theta \in [0, 2\pi]$ from

$$\frac{d\langle P_q \rangle_0}{d\theta} \bigg|_{\theta_n} = 0, \quad (10)$$

and select solutions θ_n that satisfy

$$\frac{d^2\langle P_q \rangle_0}{d\theta^2} \bigg|_{\theta_n} \neq 0. \quad (11)$$

The analytic expression for the derivatives of the function $\langle P_q \rangle_0(\theta)$ are shown in appendix A. If a solution θ_m exists which satisfies $d^2\langle P_q \rangle_0/d\theta^2|_{\theta_m} > 0$ and $\langle P_q \rangle_0(\theta_m) \leq \langle P_q \rangle_0(\theta_l) \forall \theta_l \in \theta_n$, we accept the rotation attempt $i \rightarrow q$ and $j \rightarrow p$ with rotation angle θ_m and we reject the rotation attempt otherwise. By repeating the procedure for each pair of basis orbitals ϕ_i and ϕ_j , we arrive at an orthonormal basis in which the local parities have taken up

extremal values. We then identify the orbitals ϕ_q of the resulting basis for which $\langle P_q \rangle_0 = -1 + \varepsilon$, with ε an arbitrary small, positive value, as the spin-like orbitals of the system. Basis orbitals ϕ_p with a local parity $\langle P_p \rangle_0 \simeq +1$ can be regarded as beneficial for the purpose of separating the system's spin degrees of freedom from their respective environment since they experience exclusively a transfer of an even number of particles only, such that the spin degree of freedom of electrons occupying the orbitals ϕ_p becomes insignificant. If the optimization gets stuck we found that first optimizing for minimal parities, and then optimizing the non spin-like orbitals for maximal parity we get out of local minima. In addition, we have implemented an optimization scheme using the full gradient. Currently, the pairwise optimization is typically more efficient, but this approach may help in the future to improve convergence.

D. Perturbative similarity transformation

In principle, any Hamiltonian can be completely diagonalized by means of a particular unitary transformation U . In practice, finding the particular unitary transformation U often requires a complete diagonalization of the Hamiltonian to begin with. Here we recap how a perturbative similarity transformation, namely the Schrieffer-Wolff transformation [7, 9], can be used to determine an approximate transformation operator U , or the generator S thereof, which does not diagonalize the Hamiltonian fully, but yields a block-diagonal Hamiltonian instead. These blocks consist of the orthonormal states in the Hilbert space \mathcal{H} that share a given choice of characteristics, e.g. the local particle quantum number n_i . We will denote the set of terms in the Hamiltonian that are already block-diagonal in the initial basis as H_0 . The remaining terms connect different blocks, i.e. are block-offdiagonal, and are denoted V . The complete Hamiltonian thus reads

$$H = H_0 + V. \quad (12)$$

A unitary similarity transformation of the Hamiltonian is given by

$$\tilde{H} = U^{\dagger} H U = e^{-S} (H_0 + V) e^S = e^{-S} H_0 e^S + e^{-S} V e^S, \quad (13)$$

where S is an anti-Hermitian operator. One refers to it as the generator of the Schrieffer-Wolff transformation. The key problem of the Schrieffer-Wolff transformation becomes finding the generator S such that the transformed Hamiltonian \tilde{H} becomes entirely block-diagonal. In order to arrive at an equation for S one makes use of the Campbell-Baker-Hausdorff formula to expand

$$\tilde{H} = e^S H e^{-S} = \sum_{m=0}^{\infty} \frac{1}{m!} [S, H]_m = H + [S, H] + \frac{1}{2} [S, [S, H]] + \dots, \quad (14)$$

where for generators S satisfying $\|S\| \ll \|H_0\|$, with $\|\cdot\|$ a suitable norm, one can approximate the expression as

$$\tilde{H} = H_0 + V + [S, H_0] + [S, V] + \mathcal{O}(S^2). \quad (15)$$

Considering that commutators of pairs of block-diagonal operators or pairs of block-offdiagonal operators respectively generally become block-diagonal, while the commutators of block-diagonal operators with block-offdiagonal operators become block-offdiagonal, one chooses the equation

$$[S, H_0] = -V \Leftrightarrow [H_0, S] = V, \quad (16)$$

by which one can determine the generator S which removes the block-offdiagonal terms V of the Hamiltonian. If a solution S to eq. (16) exists, one can use

$$[S, [S, H_0]] = [S, -V] = -[S, V] \notin \mathcal{O}(S^2), \quad (17)$$

to simplify the expression for the transformed Hamiltonian

$$\tilde{H} = e^{-S} (H_0 + V) e^S \simeq H_0 + \frac{1}{2} [S, V] + \mathcal{O}(S^2), \quad (18)$$

where the terms originating from $[S, V]/2$ contain the perturbative corrections arising from the consecutive application of two block-offdiagonal operators. A subsequent projection to the subspaces

$$\mathcal{P}_n = \sum_{p \in \mathcal{P}_n} |p\rangle\langle p|, \quad (19)$$

yields the block-diagonal Hamiltonian

$$\tilde{H}_{\text{block-diagonal}} = \sum_n \mathcal{P}_n \tilde{H} \mathcal{P}_n, \quad (20)$$

where n denotes the distinct blocks of the Hilbert space.

E. Symmetry specification of block-offdiagonal operators

The block-offdiagonal part of the Hamiltonian V consists of a sum of block-offdiagonal terms. These in turn comprise products of individually block-offdiagonal operators x . In the following we detail a method to decompose generic block-offdiagonal operators x into distinct components. Each of the components exclusively connects two distinct blocks of the Hilbert space \mathcal{H} , often

associated with distinct quantum numbers of a symmetry of the system. A given block-offdiagonal operator $x : \mathcal{H} \rightarrow \mathcal{H}$ satisfies

$$[H_0, x] = \varepsilon z \neq 0, \quad (21)$$

where ε denotes an arbitrary scalar and $z : \mathcal{H} \rightarrow \mathcal{H}$ an arbitrary operator. Let A be a diagonal operator in the initial basis. It can be identical to the symmetry operator differentiating the blocks of the Hilbert space, but is not required to be. One can use the spectrum of A to expand the operator x as

$$x = \sum_q x_q = \sum_q \beta_q \prod_{i \neq q} (A - a_i) x, \quad (22)$$

where the different x_q couple the target subspace associated with the eigenvalue a_q of A to other subspaces of the Hilbert space. If the operator A satisfies

$$[x, A] = 0, \quad (23)$$

then both subspaces, initial and final, coupled via x_q are specified by the eigenvalue a_q . This is possible for the fermionic creation and annihilation operators $c_{i\sigma}^\dagger$ and $c_{i\sigma}$ and is displayed in appendix B. The coefficients β_q are solutions to the equation

$$\beta_q \prod_{i \neq q} (a_q - a_i) = 1. \quad (24)$$

The symmetry-specified block-offdiagonal operators x_q satisfy

$$[x_q, x_{q'}^\dagger] \propto \delta_{qq'}, \quad (25)$$

where the operator x_q^\dagger denotes the Hermitian conjugate of the operator x_q .

F. Schrieffer-Wolff transformation as a system of linear equations for unique block-offdiagonal operators

Following the procedure outlined in Section II D we separate the Hamiltonian of the system into its block-diagonal and block-offdiagonal contributions as

$$H = H_0 + V. \quad (26)$$

The block-offdiagonal contribution V comprises each block-offdiagonal term v

$$V = \sum_{\{v\}} \alpha_v \left[\left(\prod_j o^j \prod_i x^i \right) + \left(\prod_j o^j \prod_i x^i \right)^\dagger \right] \quad (27)$$

$$= \sum_{\{v\}} \alpha_v \left[\left(\prod_{i,j} o^j \sum_{q(i)} x_{q(i)}^i \right) + \left(\prod_{i,j} o^j \sum_{q(i)} x_{q(i)}^i \right)^\dagger \right],$$

where $\prod_i x^i$ denotes sequences of individually block-offdiagonal operators, $\prod_j o^j$ denotes sequences of individually block-diagonal operators, and $x_{q(i)}^i$ denotes the symmetry-specified components of the operator x^i . We introduce a vector spaces \mathcal{V}_0^h and \mathcal{V}_0^a , for which each unique pair of Hermitian, or anti-Hermitian respectively, symmetry-specified operator sequences in V corresponds to a unique orthonormal basis vector

$$\hat{e}_v = \begin{cases} \left(\prod_j o^j \prod_i x_{q(i)}^i \right) + \left(\prod_j o^j \prod_i x_{q(i)}^i \right)^\dagger \in \mathcal{V}_0^h, \\ \left(\prod_j o^j \prod_i x_{q(i)}^i \right) - \left(\prod_j o^j \prod_i x_{q(i)}^i \right)^\dagger \in \mathcal{V}_0^a, \end{cases} \quad (28)$$

where \mathcal{V}^h denotes the Hermitian vector space and \mathcal{V}^a the anti-Hermitian vector space. We define the linear map

$$L : \begin{cases} \mathcal{V}_0^h \rightarrow \mathcal{V}_1^a \\ \mathcal{V}_0^a \rightarrow \mathcal{V}_1^h \end{cases}, \quad (29)$$

where the action of the linear map on a vector \hat{e}_v is given by

$$L \hat{e}_v = [H_0, \hat{e}_v], \quad (30)$$

where

$$\begin{cases} (L \hat{e}_v) \in \mathcal{V}_1^a & \text{if } \hat{e}_v \in \mathcal{V}_0^h \\ (L \hat{e}_v) \in \mathcal{V}_1^h & \text{if } \hat{e}_v \in \mathcal{V}_0^a \end{cases}, \quad (31)$$

with

$$\dim(\mathcal{V}_1) \geq \dim(\mathcal{V}_0), \quad (32)$$

since \mathcal{V}_1 includes additional unique operator sequences generated by $[H_0, \hat{e}_v]$. In the vector spaces \mathcal{V} we can translate equation (16) for the generator S of the Schrieffer-Wolff transformation to

$$L \vec{S} = \vec{V} \Leftrightarrow [H_0, S] = V, \quad (33)$$

with $\vec{S} \in \mathcal{V}_0^a$ and $\vec{V} \in \mathcal{V}_1^h$. Determining the generator S of the Schrieffer-Wolff transformation becomes equivalent to solving the set of linear equations (33). In general one finds

$$\text{rank}(L) \leq \dim(\mathcal{V}_0) \leq \dim(\mathcal{V}_1), \quad (34)$$

and there is consequently no unique solution \vec{S} to the set of equation (33). It is intuitive that the terms of V approximately bring about transitions between distinct eigenstates of H_0 belonging to different blocks of the Hilbert space. This is reflected by

$$[H_0, \hat{e}_v^h] = \left(\Delta E_{0,v} \prod_l o^l \right) \hat{e}_v^a, \quad (35)$$

where $\Delta E_{0,v}$ denotes the eigenvalue difference between the two eigenstates of H_0 and $\prod_l o^l$ denotes an arbitrary sequence of individually block-diagonal operators. From equations (33) and (35) we can approximate

$$\|\vec{S}\| \approx \sqrt{\sum_{\{v\}} \left(\frac{\alpha_v}{\Delta E_{0,v}} \right)^2}, \quad (36)$$

which highlights the necessity for a significant energy gap $\Delta E_{0,v}$ between the separate subspaces of the Hilbert space coupled by V in order for the series expansion of \tilde{H} to $\mathcal{O}(S^2)$ to be considered a good approximation. We consider terms v for which

$$\frac{\alpha_v^2}{|\Delta E_{0,v}|} \geq 1, \quad (37)$$

to be the resonant terms of V which should be retained in the transformed Hamiltonian \tilde{H} . To identify these resonant terms of V , we employ a singular value decomposition (SVD) of the linear map L and arrive at

$$L = U \Sigma W^\dagger = U (\Sigma_> + \Sigma_<) W^\dagger = L_{\text{gapped}} + L_{\text{resonant}}, \quad (38)$$

where $\Sigma_>$ comprises the singular values

$$\sigma_i > \frac{1}{N_v} \sum_{\{v\}} \sqrt{\alpha_v^2}, \quad (39)$$

where N_v denotes the number of terms v . We define the Moore-Penrose pseudoinverse of L that acts exclusively on the gapped, i.e. non-resonant, terms in V as

$$L_{\text{gapped}}^+ = (W \Sigma_>^+ U^\dagger), \quad (40)$$

where $\Sigma_>^+$ denotes the pseudoinverse of $\Sigma_>$. In the absence of a unique solution to (33), the closest approximate solution [32] is given by

$$\vec{S} = \left(L_{\text{gapped}}^+ \vec{V} \right) \in \mathcal{V}_0^a, \quad (41)$$

and the resulting transformed Hamiltonian reads

$$\tilde{H} = H_0 + V_{\text{resonant}} + [S, V_{\text{resonant}}] + \frac{1}{2} [S, V_{\text{gapped}}], \quad (42)$$

where $V_{\text{gapped}} = [H_0, S]$ and $V_{\text{resonant}} = (V - V_{\text{gapped}})$. The quality of the approximate transformed Hamiltonian

\tilde{H} and its respective $\tilde{H}_{\text{block-diagonal}}$ (see eq. 20) for the description of the low energy dynamics of a given system is discussed in Sections III C to III E.

In summary, we have mapped the non-linear Schrieffer-Wolff equations, as presented in the original work, [7] to a linear set of equations, see also Sec. III C. Without this representation we could not apply the Schrieffer-Wolff approach to quantum chemistry descriptions including four-index terms.

G. Full workflow

In the following we outline the steps of the workflow that we use to derive an effective spin-bath model Hamiltonian from a first principles description of a material.

a. Computation of the required system information
We start with an ab-initio electronic structure calculation [33] of the material to determine its ground state. The electronic structure method needs to be a post-Hartree-Fock or a related method, this excludes density functional theory, to capture the effect of correlations in the two-particle reduced density matrix $\rho^{(2)}$. From the electronic structure calculation we obtain the single particle basis orbitals and the corresponding one-electron and two-electron integrals which specify the Hamiltonian description. For the ground state of the calculation we compute the one-particle and two-particle reduced density matrices $\rho^{(1)}$ and $\rho^{(2)}$.

b. Determination of spin-like basis orbitals
We utilize the reduced density matrices to assign a local parity $\langle P_i \rangle_0$ to the basis orbitals ϕ_i . We then perform pairwise rotations of the basis orbitals to determine the basis in which the local parities of the basis orbitals is extremized. If there exist optimized basis orbitals ϕ_q with $\langle P_q \rangle_0 + 1 < \varepsilon$, where we typically chose $\varepsilon \leq 10^{-1}$, we proceed with the subsequent steps of the workflow. If no spin-like orbitals are found, we terminate the workflow, because the absence of spin-like orbitals also indicates the absence of relevant spin physics in the system under consideration.

c. Schrieffer-Wolff transformation of the Hamiltonian
We use our Schrieffer-Wolff transformation approach to integrate out the valid terms of the Hamiltonian that modify the electron density in the spin-like orbitals which leads to renormalized couplings of the electron spins in the spin-like orbitals to the environment. The valid terms are the ones that couple subspaces of the Hilbert space between which there exists a significant energy gap.

d. Construction of the effective spin-bath Hamiltonian
The transformed Hamiltonian \tilde{H} is projected to the particular subspace of the Hilbert space where the electron density of spin-like orbitals ϕ_q is fixed to $n_q \equiv 1$. Utilizing the identity $n_q = n_{q\uparrow} + n_{q\downarrow} \equiv 1$ fermionic operators acting on the spin-like operators are substituted with the corresponding spin operators. The resulting Hamiltonian \mathcal{PHP} is the effective spin-bath representation of

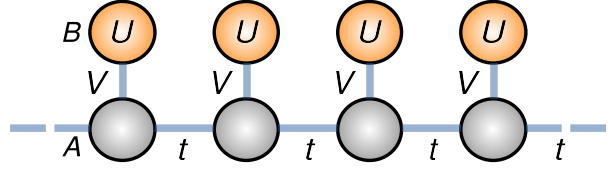


FIG. 1: Schematic representation of the lattice model described by the Hamiltonian (43). The lattice sites A_i are shown in grey. On the orange lattice sites B_i the fermions experience a strong repulsive Hubbard interaction U which energetically discourages $n_{B_i} \neq 1$. We refer to the lattice sites A_i and B_i as the initial basis of the system. The hybridization between the lattice sites A_i and A_{i+1} is given by $t < 0$. We impose periodic boundary conditions via a hybridization t between the lattice sites $A_{N=4}$ and A_1 . There is a small hybridization $0 > V > t$ between lattice sites A_i and B_i . The local Hubbard density-density interaction of strength $U \gg |t|$ is strongly repulsive. The connectivity and the coupling constants of the lattice models are chosen such that the lattice sites B_i should be good realizations of spin-like orbitals.

the material.

e. Representation on a quantum computing device (optional)
The effective spin-bath model Hamiltonian \mathcal{PHP} is re-expressed in terms of the spin operators that are realized on the specific device.

III. EXAMPLES

Here we present a selection of systems to which we have applied our methods for identifying spin-like orbitals and for deriving effective spin-bath model Hamiltonians. In Sections III A and III B we showcase the spin identification procedure for a lattice model and for a radical molecular system. In Sections III C and III D we compare our Schrieffer-Wolff transformation method with the established results for two well-known model Hamiltonians. In Section III E we then apply the complete workflow to molecular chromium bromide and discuss the accuracy of the effective spin-bath model Hamiltonians.

A. Spin-bath chain model

As a first test of the parity optimization procedure we introduce a simple lattice model. We have chosen the connectivity of the lattice sites and the coupling con-

stants such that for the lattice sites B_i an electron density $\langle n_{B_i} \rangle_0 \neq 1$ is strongly discouraged. The lattice sites B_i should consequently be good realizations of spin-like orbitals. The Hamiltonian of the lattice model reads

$$H = \sum_{i\sigma} \left(t a_{i+1\sigma}^\dagger a_{i\sigma} + V a_{i\sigma}^\dagger b_{i\sigma} + \text{h.c.} \right) \quad (43)$$

$$+ U \sum_i \left(b_{i\uparrow}^\dagger b_{i\uparrow} - \frac{1}{2} \right) \left(b_{i\downarrow}^\dagger b_{i\downarrow} - \frac{1}{2} \right),$$

where $a_{i\sigma}^\dagger$ creates a fermion of spin σ on lattice site A_i and $b_{i\sigma}^\dagger$ creates a fermion of spin σ on lattice site B_i . The lattice sites A_i and B_i form the initial basis of the system. We impose periodic boundary conditions for the lattice sites A_i . A graphic representation of the lattice model is displayed in Fig. 1. The coupling constants satisfy $U \gg |t| > |V|$ and $0 > V > t$. The repulsive Hubbard interaction on lattice sites B_i in combination with the weak hybridization between B_i and A_i places a significant energy penalty on $n_{B_i} \neq 1$. Low-energy eigenstates of the Hamiltonian should therefore satisfy $n_{B_i} \equiv 1$ and the lattice sites B_i be considered good realizations of spin-like orbitals.

We have calculated the low energy spectrum of the Hamiltonian of a chain of $M = 4$ unit cells containing $N = 8$ fermions using a numerical diagonalization method. The reduced density matrices $\rho^{(1)}$ and $\rho^{(2)}$ have been computed for the corresponding ground state $|\psi_0\rangle$. By definition [34], the eigenstates of $\rho^{(1)}$ form the natural (spin) orbital basis. We find eigenvalues $\langle n_i \rangle = 1$ of $\rho^{(1)}$ for $N_{\phi_i} = 2$ natural basis orbitals ϕ_i . These are considered two natural spin orbitals. The local parities of the natural orbitals are shown in Fig. 2a.

We find $\langle P_i \rangle_0 > 0$ for each natural basis orbital ϕ_i . This indicates that the ground state $|\psi_0\rangle$ features significant contributions from Slater determinants $|\xi\rangle$ where $n_i|\xi\rangle = 0|\xi\rangle$ or $n_i|\xi\rangle = 2|\xi\rangle$ respectively for each natural basis orbital. The average of these contributions yields $\langle n_i \rangle_0 = 1$, but the contributions $\langle \psi_0 | \xi \rangle \neq 0$ manifest themselves in strong fluctuations $|\delta n_i| \gg 0$. The lattice model highlights that the natural orbitals are generally not suitable candidates for spin-like orbitals, because they do not satisfy the necessary criterion $\delta n_i \rightarrow 0$. We point out that the original basis had already contained the spin-like lattice sites B_i . In the given example the natural orbital basis fails to be a good starting point in the search for spin-like orbitals. To test the capability of the parity optimization procedure we have used the natural orbital basis as the starting point, because we have previously found them to be sufficiently far from the optimal original basis. The results of the parity optimization are shown in Fig. 2b.

We find $N_{\phi_q} \geq 4$ orbitals ϕ_q with local parity $\langle P_q \rangle_0 \simeq -1$. These optimized orbitals ϕ_q coincide with the original lattice sites of B_i . Despite the intentionally difficult starting conditions the parity optimization procedure was able to recover the original basis featuring the lattice sites B_i that had been designed to be spin-like.

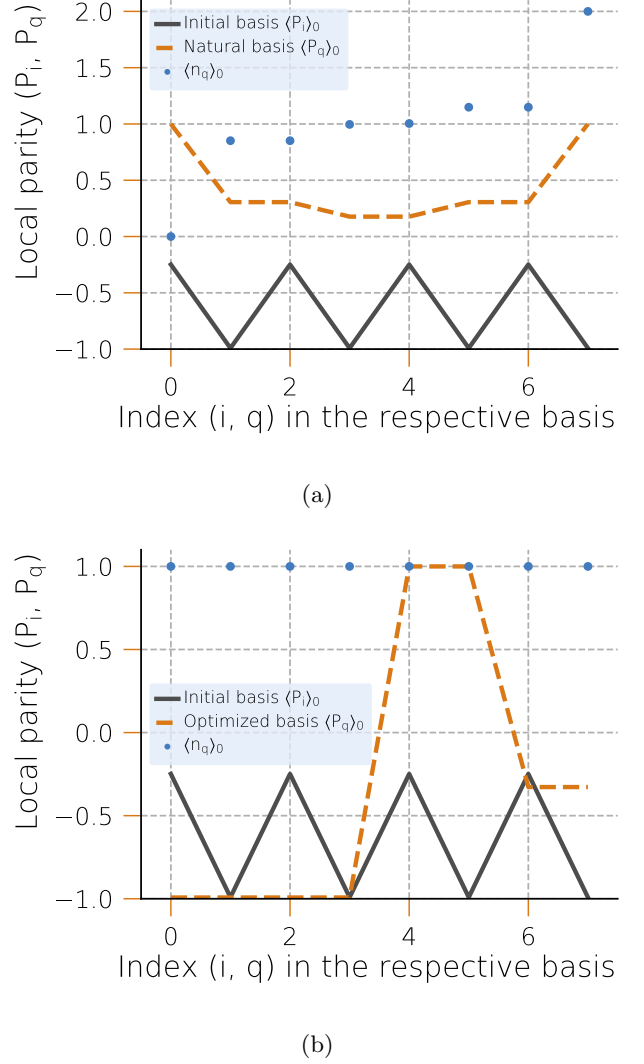


FIG. 2: Ground state expectation values of the local parity $\langle P_q \rangle_0$ of the initial basis orbitals A_i and B_i , as well as (a) the natural (spin) orbitals basis and (b) the parity optimized basis for the spin-bath chain model described by eq. (43). (a) The dark grey line shows the local parities of the original basis orbitals A_i and B_i and the dashed orange line indicates the local parities of the natural basis orbitals. The blue circles display the expectation values for the electron density $\langle n_q \rangle_0$ in the natural orbital basis. In the natural orbital basis we find $N_{\phi_q} = 2$ orbitals ϕ_q for which $\langle n_q \rangle_0 = 1$, but the respective values of the local parities $\langle P_q \rangle_0 > 0$ highlight that $|\delta n_q| \gg 0$. (b) The dashed orange line now displays the ground state local parities of the parity optimized basis orbitals. The blue circles show the expectation value for electron density $\langle n_q \rangle_0$ in these optimized basis orbitals. In the optimized basis we find $N_{\phi_q} = 4$ orbitals ϕ_q with local parity $\langle P_q \rangle_0 \simeq -1$. We also observe $\langle n_q \rangle_0 = 1$ for each orbital. The orbitals $\phi_{q \leq 3}$ of the optimized basis are considered spin-like. They coincide with the lattice sites B_i , but the ordering has been shuffled in the optimization procedure.

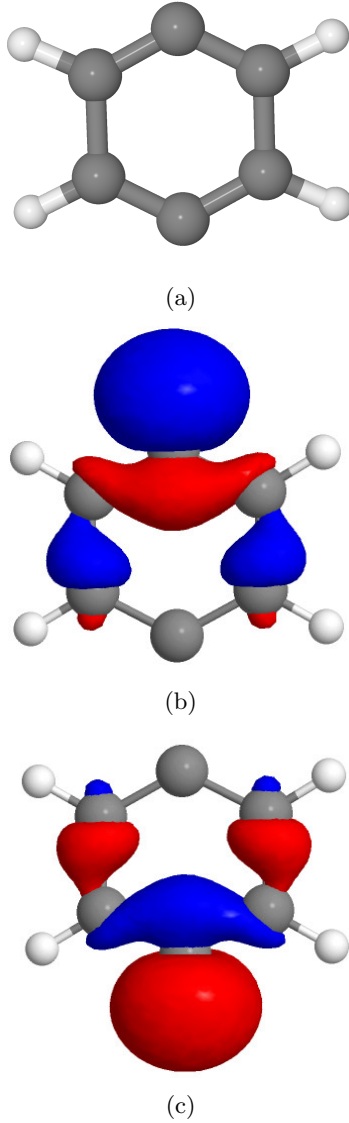


FIG. 3: (a) Molecular structure of the closed configuration of the molecule para-benzene (C₆H₄). (b) Isosurface of one spin-like orbital $\phi_{q=1}$ of para-benzene. (c) Isosurface of the other spin-like orbital $\phi_{q=2}$ of para-benzene. The colors red and blue indicate the sign of the orbital wavefunction.

B. Closed configuration of para-benzene

As a second testbed for the parity optimization procedure we have considered the molecule para-benzene C₆H₄ [35]. The molecule is depicted in Fig. 3a. In its singlet configuration para-benzene is known to feature two spin-like orbitals that are non-trivial linear combinations of the original basis orbitals [36]. The complete active space self-consistent field (CASSCF) [33, 37–39] method was used to compute the reduced density matrices $\rho^{(1)}$ and $\rho^{(2)}$ in the ground state. CASSCF wave function is

constructed as a linear combination of all Slater determinants obtained by distribution of N electrons into M orbitals, which constitute the (N, M) active space, that is N particles on M spinful orbitals are treated within their full Hilbert space, while the remaining orbitals are treated using a self consistent field approximation. Energy is obtained variationally, being minimized wrt. both active orbitals and Slater determinant coefficients. The orbital basis set comprises $N_{\phi_i} = 62$ CASSCF canonical molecular orbitals of which $N_{\phi_{i,a}} = 12$ orbitals are selected as active containing 12 electrons, giving rise to (12, 12) active space. The Hamiltonian description of the molecule in the molecular orbital basis reads

$$H = \sum_{ij\sigma\sigma'} t_{ij}^{\sigma\sigma'} c_{i\sigma}^\dagger c_{j\sigma'} + \sum_{ijkl\sigma\sigma'} V_{ijkl}^{\sigma\sigma'} c_{i\sigma}^\dagger c_{j\sigma'}^\dagger c_{k\sigma'} c_{l\sigma}, \quad (44)$$

where the one-electron integrals $t_{ij}^{\sigma\sigma'}$ and two-electron integrals $V_{ijkl}^{\sigma\sigma'}$ have been determined as part of an ab-initio calculation. The parity optimization procedure was performed for two sets of initial basis orbitals. The first set contained all $N_{\phi_i} = 62$ basis orbitals of the CASSCF calculation. The second set was restricted to the active $N_{\phi_i} = 12$ orbitals ϕ_i with local parity $\langle P_i \rangle_0 < 9.5 \times 10^{-1}$, which coincides with the active space of the CASSCF calculation. The local parities in the initial and the optimized basis are displayed in Fig. 4.

The differences between the complete and reduced basis sets are insignificant when only considering the orbitals of smallest local parity after optimization. Discrepancies between the two optimizations can be observed for basis orbitals of larger local parity. In this case the access to the complete set of basis orbitals allows for further reduction of the local parity of some basis orbitals in the optimization. After parity optimization we identify two basis orbitals ϕ_q for which the local parity takes the value $\langle P_q \rangle_0 \simeq -0.94$. This is sufficiently small a value of the local parity to be considered spin-like. The local parities of the remaining basis orbitals are significantly, larger i.e. $\langle P_p \rangle_0 > -0.5$. The two spin-like orbitals ϕ_q are the linear combinations

$$\phi_q(\vec{r}) \simeq \frac{1}{\sqrt{2}} [\phi_a(\vec{r}) \pm \phi_b(\vec{r})], \quad (45)$$

of two specific CASSCF canonical molecular orbitals ϕ_a and ϕ_b of the original basis. This is consistent with results from previous studies of the closed configuration of para-benzene [36]. An isosurface image of the two spin-like orbitals ϕ_q is displayed in figures 3b and 3c.

C. Single impurity Anderson model

The intuitive first application example for our proposed Schrieffer-Wolff transformation approach is the single impurity Anderson model (SIAM) [40]. It is the model Hamiltonian for which this type of perturbative similarity transformation was originally proposed by

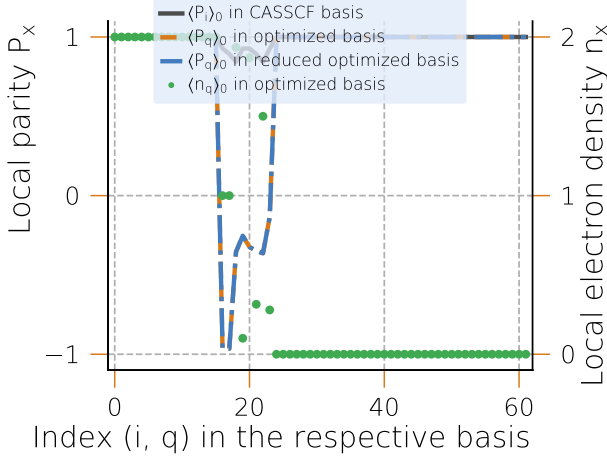


FIG. 4: Ground state local parities $\langle P_i \rangle_0$ of the basis orbitals of para-benzene (C_6H_4) in the initial CASSCF canonical molecular orbitals basis (dark grey line) and the two different parity optimized bases (dashed orange and blue). The local parities $\langle P_i \rangle_0$ of the original atomic basis orbitals each satisfy $\langle P_i \rangle_0 > 8.5 \times 10^{-1}$, so the initial basis orbitals are not considered spin-like. The local parities $\langle P_q \rangle_0$ of the basis orbitals ϕ_q in the optimized basis, where the full set of $N = 62$ orbitals has been optimized, are shown in orange. The resulting local parities $\langle P_q \rangle_0$, where the subset of $N = 12$ basis orbitals ϕ_i with initial local parity $\langle P_i \rangle_0 < 9.5 \times 10^{-1}$ has been optimized, are displayed in blue. The electron densities in the optimized basis orbitals is shown as green circles. The restricted set turns out to be equivalent to the active space of the CASSCF calculation used to obtain the reduced density matrices $\rho^{(1)}$ and $\rho^{(2)}$. The local parity $\langle P_q \rangle_0 \simeq -9.4 \times 10^{-1}$ of two specific optimized basis orbitals ϕ_q is sufficiently small for the criteria $\langle n_q \rangle_0 \equiv 1$ and $|\delta n_q| \simeq 0$ to be simultaneously fulfilled. The isosurfaces of these spin-like orbitals are displayed in Figs. 3b and 3c.

Schrieffer and Wolff. The generator of the transformation and the transformed Hamiltonian are both known analytically. The SIAM describes a localized magnetic moment in a system of non-interacting electrons. The SIAM Hamiltonian reads

$$H = \sum_{\sigma} \left[-t \sum_{i=1}^N \left(c_{i,\sigma}^\dagger c_{i-1,\sigma} + \text{h.c.} \right) - V_0 \left(d_{\sigma}^\dagger c_{0,\sigma} + c_{0,\sigma}^\dagger d_{\sigma} \right) \right. \\ \left. + U \left(d_{\uparrow}^\dagger d_{\uparrow} - \frac{1}{2} \right) \left(d_{\downarrow}^\dagger d_{\downarrow} - \frac{1}{2} \right) \right], \quad (46)$$

where d_{σ}^\dagger creates an electron with spin σ on the impurity site and $c_{i,\sigma}^\dagger$ creates an electron of spin σ on the lattice

site i of the remainder of the system. If one identifies

$$H_0 = -t \sum_{i=1,\sigma}^N \left(c_{i,\sigma}^\dagger c_{i-1,\sigma} + \text{h.c.} \right) \\ + U \left(d_{\uparrow}^\dagger d_{\uparrow} - \frac{1}{2} \right) \left(d_{\downarrow}^\dagger d_{\downarrow} - \frac{1}{2} \right) \quad (47)$$

$$V = -V_0 \sum_{\sigma} \left(d_{\sigma}^\dagger c_{0,\sigma} + c_{0,\sigma}^\dagger d_{\sigma} \right), \quad (48)$$

the canonical transformation by Schrieffer and Wolff [7, 41, 42] yields the Hamiltonian

$$\tilde{H} = - \sum_{k,k' \sigma \sigma'} J_{kk'} \left(d_{\sigma}^\dagger \vec{c}_{k \sigma} \cdot \vec{c}_{k' \sigma'} \right) \\ + \sum_{k \sigma} \left(W_{kk} + \frac{J_{kk}}{2} d_{\bar{\sigma}}^\dagger d_{\bar{\sigma}} \right) c_{k \sigma}^\dagger c_{k \sigma} \\ + \sum_{kk' \sigma} \frac{J_{kk'}}{4} c_{k \bar{\sigma}}^\dagger c_{k' \bar{\sigma}}^\dagger d_{\sigma} d_{\sigma} + \text{h.c.} + \sum_{k \sigma} \varepsilon_k c_{k \sigma}^\dagger c_{k \sigma}, \quad (49)$$

where the parameters

$$V_k \propto V_0, \quad (50)$$

$$\varepsilon_k = -2t \cos k, \quad (51)$$

are the consequence of a Fourier transformation to momentum space $k = \frac{1}{N+1}, \dots, \frac{N\pi}{N+1}$, while the effective coupling constants

$$J_{k'k} = V_{k'} V_k \left(\frac{1}{\varepsilon_k - \frac{U}{2}} + \frac{1}{\varepsilon_{k'} - \frac{U}{2}} - \frac{1}{\varepsilon_k + \frac{U}{2}} - \frac{1}{\varepsilon_{k'} + \frac{U}{2}} \right), \quad (52)$$

$$W_{k'k} = \frac{V_{k'} V_k}{2} \left(\frac{1}{\varepsilon_k + \frac{U}{2}} + \frac{1}{\varepsilon_{k'} + \frac{U}{2}} \right), \quad (53)$$

are the result of the Schrieffer-Wolff transformation. A subsequent projection \mathcal{P} of the Hamiltonian \tilde{H} to the subspace of the Hilbert space in which the impurity site is singly occupied yields the Kondo Hamiltonian [43]

$$\mathcal{P} \tilde{H} \mathcal{P} = \sum_{k \sigma} \varepsilon_k c_{k \sigma}^\dagger c_{k \sigma} - \sum_{kk' \sigma \sigma'} J_{k'k} \vec{S}_d \cdot \vec{c}_{k' \sigma}^\dagger \vec{c}_{k \sigma}, \quad (54)$$

where the magnetic impurity is coupled to the electrons in the lead via its spin degree of freedom $\vec{S}_d = (S_d^x, S_d^y, S_d^z)$ only.

We have studied a SIAM Hamiltonian of with 9 lattice sites for the lead and an additional site representing the magnetic impurity and a hybridization between lead and impurity $V_0/t = 1/4$. The hybridization t between lead lattice sites represents the energy scale of the system. We have fixed the electron number $N_{\text{electrons}} = 10$ and $\sum_i \sigma_i^z = 0$ to perform a ground state computation using a numerical diagonalization method for a range of impurity interaction strength values $3 \leq U/t \leq 40$. We have calculated the local parity $\langle P_d \rangle_0$ of the impurity site in the

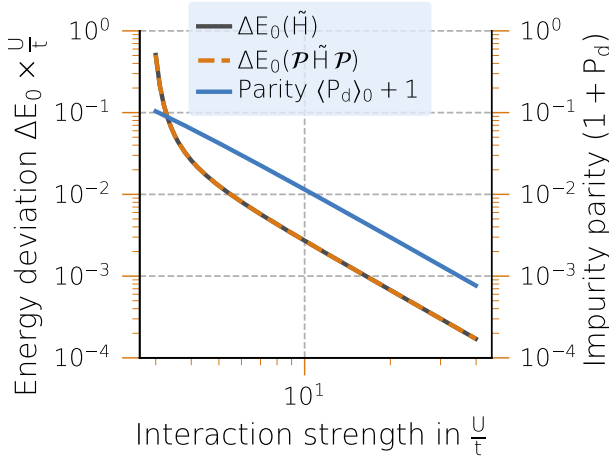


FIG. 5: Rescaled ground state energy difference $U \times \Delta E_0/t = U \times |E_0^{(\mathcal{P})\tilde{H}(\mathcal{P})} - E_0^H|/t$ between the ground state of the SIAM Hamiltonian and the transformed Hamiltonians \tilde{H} and $\mathcal{P}\tilde{H}\mathcal{P}$ as a function of the interaction strength U/t . The dark grey line represents the scaled energy difference for the transformed Hamiltonian \tilde{H} . The dashed orange displays $U \times \Delta E_0/t$ for the effective Hamiltonian $\mathcal{P}\tilde{H}\mathcal{P}$ where the impurity site is restricted to single occupancy $n_d \equiv 1$. The solid blue line displays the local parity $\langle P_d \rangle_0$ of the impurity site in the true ground state for each value of the interaction strength U/t .

ground state. We have used our Schrieffer-Wolff transformation approach to numerically determine the Hamiltonians \tilde{H} and $\mathcal{P}\tilde{H}\mathcal{P}$ for each value of the interaction strength U/t and have compared them with the established and analytic results (50) and (54). The numerical results match the analytic expressions exactly. We have also calculated the discrepancy $\Delta E_0 = |E_0^{(\mathcal{P})\tilde{H}(\mathcal{P})} - E_0^H|$ between the ground state energies E_0 of the SIAM Hamiltonian H (47) and the energy of respective ground states of the transformed Hamiltonians \tilde{H} and $\mathcal{P}\tilde{H}\mathcal{P}$. The ground state local parity $\langle P_d \rangle_0$ of the magnetic impurity and the rescaled ground energy discrepancies $U\Delta E_0/t$ as a function of the interaction strength U/t are shown in Fig. 5.

For values of the interaction strength $U/t \leq 4$, we observe several pronounced energy differences between the SIAM ground states and the ground states of the transformed and effective Hamiltonians. In this weak interaction regime, the chemical potential of the impurity lies within the bandwidth $D = 4t$ of the tight-binding chain representing the remainder of the system. There is then no energy gap between the subspace of the Hilbert space where the impurity is singly occupied and the rest of the Hilbert space. In the absence of an energy gap, limiting the series expansion (14) to first order in S is not a justi-

fied approximation. For values of the interaction strength $U/t > 4$ we observe a decrease of the energy discrepancy ΔE_0 of the ground state energies of the SIAM Hamiltonian and the transformed and effective Hamiltonians respectively as a power-law $(U/t)^{-\alpha}$ of the interaction strength with an exponent $\alpha > 2$. The energy discrepancy quickly becomes small with respect to the energy scale t and we find $\Delta E_0/t \rightarrow 0$ for $U/t \rightarrow \infty$. For the ground state local parity on the impurity site we observe $7 \times 10^{-2} > \langle P_d \rangle_0 + 1 > 3 \times 10^{-2}$ in the regime $U/t \leq 4$. For larger values of the interaction strength $U/t > 4$ we find that the local parity of the impurity site approximates a polynomial function $(\langle P_d \rangle_0 + 1)(U/t) \propto (U/t)^{-\beta}$ with the exponent $\beta \approx \alpha - 1$. The local parity of the impurity site appears to be a good indicator of quality of the approximation (15) if \tilde{H} is supposed to become block-diagonal in the subspaces of the Hilbert space with different particle number n_d on the impurity site. This supports our claim that a local parity $(\langle P_d \rangle_0 + 1) \rightarrow 0$ signals that the corresponding site can be represented as a spin degree of freedom and that $\mathcal{P}\tilde{H}\mathcal{P}$ is then a good effective Hamiltonian to describe the low-energy spin dynamics of the system. The energy discrepancy ΔE_0 is identical for both \tilde{H} and $\mathcal{P}\tilde{H}\mathcal{P}$. In the case of the SIAM Hamiltonian the Schrieffer-Wolff transformation yields a Hamiltonian \tilde{H} that does no longer couple the distinct subspaces characterized by $n_d = 1$ and $n_d \neq 1$. We find that our Schrieffer-Wolff transformation method recovers the analytically known results and that the ground state of effective Hamiltonian $\mathcal{P}\tilde{H}\mathcal{P}$ approaches the true ground state as $U/t \rightarrow \infty$ at a rate faster than $(U/t)^{-1}$.

D. Disordered Fermi-Hubbard model

Another significant model Hamiltonian, for which the analytic expression for the Schrieffer-Wolff transformed Hamiltonian is known, is the Fermi-Hubbard model [44, 45]. It is translation invariant and describes the electrons in orbitals with small nearest-neighbor hybridizations t where electrons occupying the same orbital exert a density-density interaction U on each other. In the limit $U/t \rightarrow \infty$ and $N_{\text{electrons}}/N_{\text{orbitals}} = 1$ (half filling) the transformed Hamiltonian \tilde{H} reduces to the well-known Heisenberg model of interacting spins [11, 16]. Here, we present the Schrieffer-Wolff transformation for the disordered Fermi-Hubbard (dFH) chain. Its Hamiltonian is given by

$$H = \sum_{i=1}^N \sum_{\sigma} \left[\varepsilon_i c_{i,\sigma}^\dagger c_{i,\sigma} - t \left(c_{i,\sigma}^\dagger c_{i-1,\sigma} + \text{h.c.} \right) \right] \quad (55)$$

$$+ U \sum_{i=1}^N \left(c_{i\uparrow}^\dagger c_{i\uparrow} - \frac{1}{2} \right) \left(c_{i\downarrow}^\dagger c_{i\downarrow} - \frac{1}{2} \right),$$

where the values ε_i have been randomly drawn from a normal distribution of width $\sigma = t/2$. The corresponding Hamiltonian after Schrieffer-Wolff transforma-

tion and projection to the subspace of the Hilbert space where $\sum_{\sigma} c_{i\sigma}^{\dagger} c_{i\sigma} = 1$ for every site i of the chain reads

$$\mathcal{P}\tilde{H}\mathcal{P} = \sum_{i=1}^N J_i \vec{S}_i \cdot \vec{S}_{i-1} + \sum_{i=1}^N \varepsilon_i, \quad (56)$$

where $\vec{S}_i = (S_i^x, S_i^y, S_i^z)$ denotes the spin operator acting on the electron spin of the electron located on chain site i and the coupling constants $J_i = \frac{4t^2}{U} + \delta_i$ feature small local renormalizations δ_i caused by the disorder.

We have examined a disordered Fermi-Hubbard Hamiltonian of length $N = 10$ chain sites and periodic boundary conditions $c_{i=0,\sigma} = c_{i=N,\sigma}$. The hybridization t between chain sites represents the energy scale of the system. We have fixed the electron number $N_{\text{electrons}} = 10$ and $\sum_i \sigma_i^z = 0$ to perform a ground state computation using a numerical diagonalization method for a range of repulsive Hubbard interaction strength values $3 \leq U/t \leq 40$. We have computed the average local parity $(\overline{P}_i)_0 + 1$ of the chain sites in the ground state. We have used our Schrieffer-Wolff transformation approach to numerically determine the Hamiltonians \tilde{H} and $\mathcal{P}\tilde{H}\mathcal{P}$ for each value of the interaction strength U/t and have compared them with the established result (56). The numerical results match the analytic expressions exactly. We have again calculated the discrepancy ΔE_0 between the ground state energies E_0 of the dFH Hamiltonian H (55) and the energy of respective ground states of the transformed Hamiltonians \tilde{H} and $\mathcal{P}\tilde{H}\mathcal{P}$. The ground state average local parity $(\overline{P}_i)_0 + 1$ of the chain sites and the rescaled ground energy differences $U\Delta E_0/t$ as a function of the interaction strength U/t are displayed in Fig. 6.

For values of the interaction strength $U/t \leq 10$, we observe a significant energy difference ΔE_0 for both \tilde{H} and $\mathcal{P}\tilde{H}\mathcal{P}$ which is decreasing with U/t at an increasing rate faster than $(U/t)^{-1}$. At values $U/t > 10$ the energy difference becomes small with respect to the energy scale t and is approaching $\Delta E_0 \rightarrow 0$ for $U/t \rightarrow \infty$ at a rate faster than $(U/t)^{-2}$. Similarly we find average local parity $(\overline{P}_i)_0 + 1 > 10^{-1}$ for $U/t \leq 10$. This highlights that the chain sites cannot be considered good realizations of spin degrees of freedom in this regime. The transformed Hamiltonian \tilde{H} can consequently not be considered a good approximation to the Hamiltonian H (55). This is supported by the respective values of $\Delta E_0/t \geq 1$. As $(\overline{P}_i)_0 + 1)(U/t) \ll 10^{-1}$ for $U/t > 10$ we also observe that the transformed Hamiltonian becomes an ever better approximation of the original dFH Hamiltonian and $\Delta E_0/t \ll 1$. For the disordered Fermi-Hubbard Hamiltonian we again find that our Schrieffer-Wolff transformation method recovers the analytically known results. The ground state of effective Hamiltonian $\mathcal{P}\tilde{H}\mathcal{P}$ approaches the true ground state as $U/t \rightarrow \infty$ at a rate faster than $(U/t)^{-1}$ and the crossover at which $\mathcal{P}\tilde{H}\mathcal{P}$ becomes a good description of the low-energy dynamics of the model is characterized by $(\overline{P}_i)_0 + 1 < 10^{-1}$. We

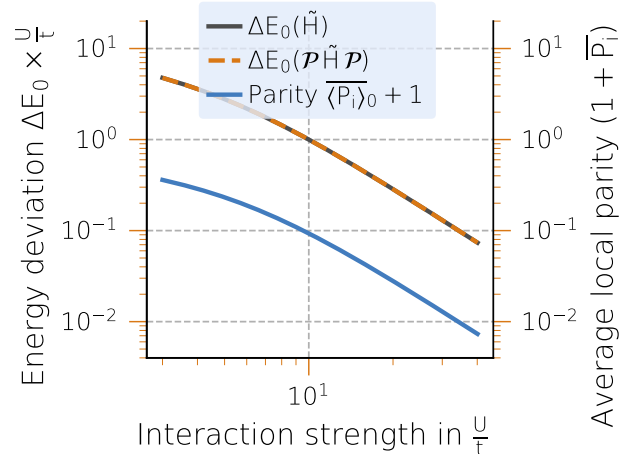


FIG. 6: Rescaled energy difference $U \times \Delta E_0/t$ between the true ground state of the disordered Fermi-Hubbard chain and the ground states of \tilde{H} (dark grey) and of the Heisenberg Hamiltonian $\mathcal{P}\tilde{H}\mathcal{P}$ (dashed orange), where the chain sites are replaced with local spin degrees of freedom, and the true ground state. The blue line displays the average local parity $(\overline{P}_i)_0 = \frac{1}{N} \sum_{i=1}^N \langle P_i \rangle_0$ of the individual chain sites i in the ground state.

note that the Schrieffer Wolff transformation renormalizes the local disorder potentials.

E. Molecular Chromium bromide

An interesting testbed for our spin mapping approach, is the class of 2D magnetic materials, which have recently been discovered experimentally[46, 47]—seemingly in contradiction to the Mermin-Wagner theorem. A common approach to study 2D magnetic materials from first principles is to perform a so-called “DFT+U” calculation, followed by a Wannierization and the extraction of a *classical* Heisenberg-like spin model from the resulting tight-binding description of the material (cf. [48] for a recent study on Chromium tri-halides). The spin mapping proposed in this work represents an alternative for extracting the effective spin model. The key difference to the aforementioned workflow to extract effective spin models using DFT is: 1) A correlated quantum-chemistry (wave-function) approach is used to determine a basis set featuring spin-like orbitals. 2) The Schrieffer–Wolff transformation starts from full description not relying on the approximate multi-reference method used to determine the spin-like orbitals. 3) The Hamiltonian resulting from the Schrieffer-Wolff transformation is still a quantum mechanical Hamiltonian, i.e., the classical limit is not implied by the spin mapping approach.

Let us point out that we neither claim that a full quantum mechanical treatment of the effective spin model is

required for getting an accurate spin model for (ferromagnetic) transition-metal tri-halides, nor that a correlated method is required for the electronic-structure calculation (however, standard DFT, without “+U”, is not sufficient to capture the localized Chromium d -orbitals). We would also like to note that the main purpose of the multi reference calculation is the determination of the spin orbitals, i.e. the single particle basis. We can use hints from multi reference methods to restrict the application of the Schrieffer-Wolff transformation to a subset of all orbitals, but this step is not essential.

As a minimal model for the CrBr_3 solid, we consider a minimal cluster, comprised of a single Chromium atom, cut out from the periodic structure, together with an octahedron of six Bromide atoms coordinating the transition metal. To study the spin mapping approach for inter-Chromium couplings larger clusters must be considered, which is beyond the scope of the present work. As a first step towards studying chromium bromide CrBr_3 we hence study a CrBr_6^{3-} cluster to test the applicability of our approach.

We initially perform a series of electronic structure calculations using the def2-QZVP basis set to generate the information necessary for a search of the active space of orbital basis of the system. We have used the Active Space Finder (ASF), [49] an open-source to assist the user in the selection of an active space. As expected, five Chromium d -orbitals and p -orbitals from the outer Shell of Bromide are suggested by the ASF and the active space contains $N_{\phi_i} = 9$ basis orbitals. We have performed a CASSCF calculation using the previously identified orbitals as the active space to compute the reduced density matrices $\rho^{(1)}$ and $\rho^{(2)}$ for the CASSCF ground state. From this CASSCF calculation we have also obtained the one-electron $t_{ij}^{\sigma\sigma'}$ and two-electron integrals $V_{ijkl}^{\sigma\sigma'}$ in the active space. We can write the Hamiltonian description of the active space of chromium bromide as

$$H = \sum_{ij\sigma\sigma'} t_{ij}^{\sigma\sigma'} c_{i\sigma}^\dagger c_{j\sigma'} + \sum_{ijkl\sigma\sigma'} V_{ijkl}^{\sigma\sigma'} c_{i\sigma}^\dagger c_{j\sigma'}^\dagger c_{k\sigma'} c_{l\sigma}, \quad (57)$$

where $c_{i\sigma}^\dagger$ creates an electron with spin σ in the orbital ϕ_i of the active space. Using the reduced density matrices we have performed a parity optimization of the basis orbitals of the active space. Here, we first ran a parity minimization procedure of the entire basis and identified $N_{\phi_q} = 3$ spin-like orbital with respective parities $\langle P_q \rangle_0 \leq -9.94 \times 10^{-1}$. In a subsequent optimization run have maximized the local parities of the remaining basis orbitals. The local parities of the initial basis orbitals ϕ_i and the optimized basis orbitals ϕ_q are shown together with the average electron density $\langle n_q \rangle_0$ in Fig. 7.

We find that three orbitals ϕ_i of the original basis already have smaller local parities $\langle P_i \rangle_0 \leq -5.53 \times 10^{-1}$. The spin-like orbitals ϕ_q of the optimized basis feature significant contributions by these initial basis orbitals

$i = \{4, 6, 7\}$. The orbitals ϕ_q read

$$\begin{aligned} \phi_{q=0} &= -0.81 \phi_7 - 0.49 \phi_8 + 0.20 \phi_5 + \dots, \\ \phi_{q=1} &= -0.86 \phi_4 - 0.20 \phi_7 + \dots, \\ \phi_{q=2} &= +0.95 \phi_6 - 0.26 \phi_1 + \dots, \end{aligned} \quad (58)$$

where \dots denotes minor contributions from the other basis orbitals ϕ_i .

We have performed a first numerical diagonalization computation of the $n = 20$ lowest energy eigenstates of the effective Hamiltonian $\mathcal{P}_0 H \mathcal{P}_0$, which acts exclusively on the subspace of the Hilbert space characterized by $n_i \equiv 1$, for $i \in \{4, 6, 7\}$. In the calculation we have fixed $N_{\text{electrons}} = 9$ and $\sum_i \sigma_i^z = 3$. Subsequently, the Hamiltonian H was transformed to the parity-optimized orbital basis and a second numerical diagonalization with the same constraints for electron number and total spin σ^z was performed. For each of the $n = 20$ lowest energy eigenstates of the Hamiltonian H we have computed the local parity $\langle P_{q \in \mathcal{S}} \rangle_n$ of the orbitals initially identified as spin-like $\phi_{q \in \mathcal{S}}$, where $\mathcal{S} = \{0, 1, 2\}$. We have projected the Hamiltonian H in the parity-optimized basis to the subspace of the Hilbert space where the number of electrons in the spin-like orbitals $\phi_{q \in \mathcal{S}}$ is fixed $n_{q \in \mathcal{S}} \equiv 1$. Using the same numerical diagonalization method we have computed the $n = 20$ lowest energy eigenstates of this projected Hamiltonian $\mathcal{P}H\mathcal{P}$. For the Schrieffer-Wolff transformation we have introduced a cut-off $c = 10^{-5}$ Hartree for the constituent terms of the Hamiltonian. Hamiltonian terms of coupling constant $|h|$ smaller than the cutoff have been neglected in the calculation of the transformed Hamiltonian \tilde{H} to limit the memory consumption of the computation. The singular value decomposition in our Schrieffer-Wolff transformation approach was performed using a Krylov subspace method with a maximum dimension of the subspace $\dim(\mathcal{K}) = 4000$. The size of the vector spaces \mathcal{V} depends on the choice of the cutoff. For chromium bromide we determine $\dim(\mathcal{V}_0)(c) = 8760$ for the initial vector space and $\dim(\mathcal{V}_1)(c) = 3.6 \times 10^6$ for the target vector space. The prevalent interaction terms in the transformed Hamiltonian read

$$\begin{aligned} \tilde{H} = & \sum_{q \in \mathcal{S}, \sigma} t_{qq}^{\sigma\sigma} c_{q\sigma}^\dagger c_{q\sigma} + \sum_{qp \in \mathcal{S}} h_{qp} \vec{S}_q \cdot \vec{S}_p \\ & + \sum_{q \in \mathcal{S}, ij \in \bar{\mathcal{S}}, \sigma\sigma'} h_{qqij}^{\sigma\sigma'} c_{q\sigma}^\dagger c_{q\sigma'} c_{i\sigma'}^\dagger c_{j\sigma} \\ & + \sum_{ij \in \bar{\mathcal{S}}, \sigma\sigma'} t_{ij}^{\sigma\sigma'} c_{i\sigma}^\dagger c_{j\sigma'} + \sum_{ijkl \in \bar{\mathcal{S}}, \sigma\sigma'} V_{ijkl}^{\sigma\sigma'} c_{i\sigma}^\dagger c_{j\sigma'}^\dagger c_{k\sigma'} c_{l\sigma} \\ & + \dots, \end{aligned} \quad (59)$$

and amount to $N_{|h|>c} = 41239$ terms with a coupling constant $|h| > c$. The projection of the transformed Hamiltonian to the subspace of the Hilbert space, in which the spin-like orbitals $\phi_{q \in \mathcal{S}}$ are replaced with spin degrees of

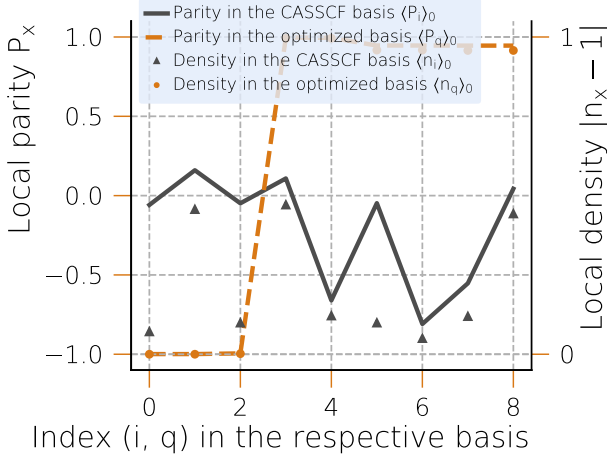


FIG. 7: Local parities of the active space basis orbitals of molecular chromium bromide CrBr_6^{3-} in the CASSCF ground state. The dark grey line displays the CASSCF ground state local parities of the CASSCF canonical molecular orbitals, which form the active space of the system. The dashed orange line indicates the ground state local parities of the optimized basis orbitals ϕ_q and the orange circles show the expectation value for the local electrons density of basis orbitals ϕ_q in the ground state. The dark gray triangles indicate the expectation values for local electron density in the original CASSCF basis orbitals. In the optimized basis there exist three basis orbitals that feature local parities $\langle P_q \rangle_0 < -0.994$, indicating good realizations of three spin degrees of freedom.

freedom, is given by

$$\begin{aligned} \mathcal{P}\tilde{H}\mathcal{P} = & \sum_{qp \in \mathcal{S}} h_{qp} \vec{S}_q \cdot \vec{S}_p + \sum_{q \in \mathcal{S}, ij \in \mathcal{S}, \sigma\sigma'} h_{qij}^{\sigma\sigma'} \vec{S}_q \cdot c_{i\sigma}^\dagger \vec{\sigma} c_{j\sigma'} \\ & + \sum_{ij \in \mathcal{S}, \sigma\sigma'} t_{ij}^{\sigma\sigma'} c_{i\sigma}^\dagger c_{j\sigma'} \\ & + \sum_{ijkl \in \mathcal{S}, \sigma\sigma'} V_{ijkl}^{\sigma\sigma'} c_{i\sigma}^\dagger c_{j\sigma'}^\dagger c_{k\sigma'} c_{l\sigma} \\ & + \dots, \end{aligned} \quad (60)$$

where $\vec{S}_q = (S_q^x, S_q^y, S_q^z)$ and $\vec{\sigma} = (\sigma_{\sigma'\sigma}^x, \sigma_{\sigma'\sigma}^y, \sigma_{\sigma'\sigma}^z)$.

We have calculated the low energy spectrum of \tilde{H} and $\mathcal{P}\tilde{H}\mathcal{P}$ using a numerical diagonalization method and with the same set of constraints for the quantum numbers. The low-energy spectra from numerical diagonalization calculations of the five different Hamiltonian representations are displayed in Fig. 8 (a).

We observe that the ground state energies of the effective Hamiltonians $\mathcal{P}\mathcal{H}\mathcal{P}$, \tilde{H} , and $\mathcal{P}\tilde{H}\mathcal{P}$ are within a fraction of a Hartree from the true ground state energy

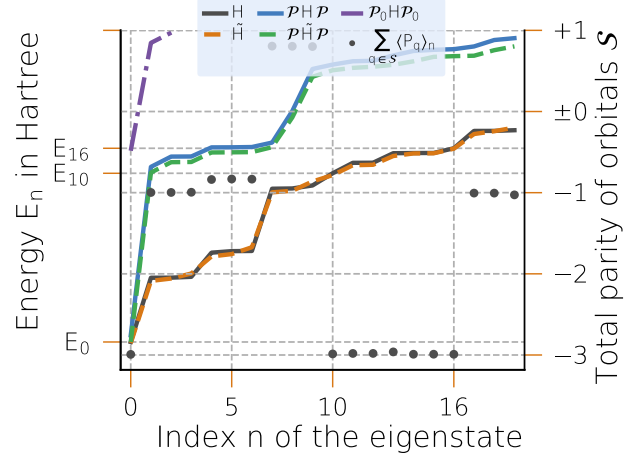


FIG. 8: Low energy spectra of the active space Hamiltonians of molecular chromium bromide CrBr_6^{3-} . The dark grey line shows the eigenenergies of the $n = 20$ lowest eigenstates of the original active space Hamiltonian H . We display the corresponding eigenenergies of the effective Hamiltonian $\mathcal{P}\mathcal{H}\mathcal{P}$ (solid blue), projected onto the subspace of the Hilbert space where the spin-like orbitals are restricted to single occupancy, the transformed Hamiltonian \tilde{H} (dashed orange), and the effective Hamiltonian $\mathcal{P}\tilde{H}\mathcal{P}$ (dashed green) acting on the subspace \mathcal{P} in which the fermionic degrees of freedom in the spin-like orbitals have been substituted with spin degree of freedom. The low energy spectrum of the effective Hamiltonian $\mathcal{P}_0 H \mathcal{P}_0$, acting only on the subspace characterized by $n_i \equiv 1$ for the CASSCF canonical orbitals $i \in \{4, 6, 7\}$, is shown in purple. The total local parity of the spin-like orbitals $\sum_{q \in \mathcal{S}} \langle P_q \rangle_n$ measured for the lowest $n = 20$ eigenstates $|n\rangle$ of the original fermionic Hamiltonian H is displayed as grey circles.

E_0^H of the original fermionic Hamiltonian H . It is noteworthy that the ground state energy $E_0^{\mathcal{P}\tilde{H}\mathcal{P}}$ of the effective spin-bath Hamiltonian $\mathcal{P}\tilde{H}\mathcal{P}$ deviates from the true ground state energy only on the order of $\mu\text{Hartree}$. The respective energy differences amount to

$$\begin{aligned} \Delta E_0^{\mathcal{P}\tilde{H}\mathcal{P}} &= (E_0^H - E_0^{\mathcal{P}\tilde{H}\mathcal{P}}) \simeq 2 \times 10^{-5} \text{ Hartree} \\ &< (E_0^H - E_0^{\tilde{H}}) \simeq 2 \times 10^{-3} \text{ Hartree} \\ &< (E_0^H - E_0^{\mathcal{P}\mathcal{H}\mathcal{P}}) \simeq 8 \times 10^{-3} \text{ Hartree}. \end{aligned}$$

In contrast, we find a significantly larger energy discrepancy $\Delta E_0^{\mathcal{P}_0 H \mathcal{P}_0} = (E_0^H - E_0^{\mathcal{P}_0 H \mathcal{P}_0}) \simeq 2 \times 10^{-1}$ Hartree for the naive effective spin-bath Hamiltonian $\mathcal{P}_0 H \mathcal{P}_0$.

At first glance, we observe significant energy differences between the original fermionic Hamiltonian H and the effective spin-bath Hamiltonians $\mathcal{P}\mathcal{H}\mathcal{P}$ and $\mathcal{P}\tilde{H}\mathcal{P}$ for the excited states, while the transformed fermionic

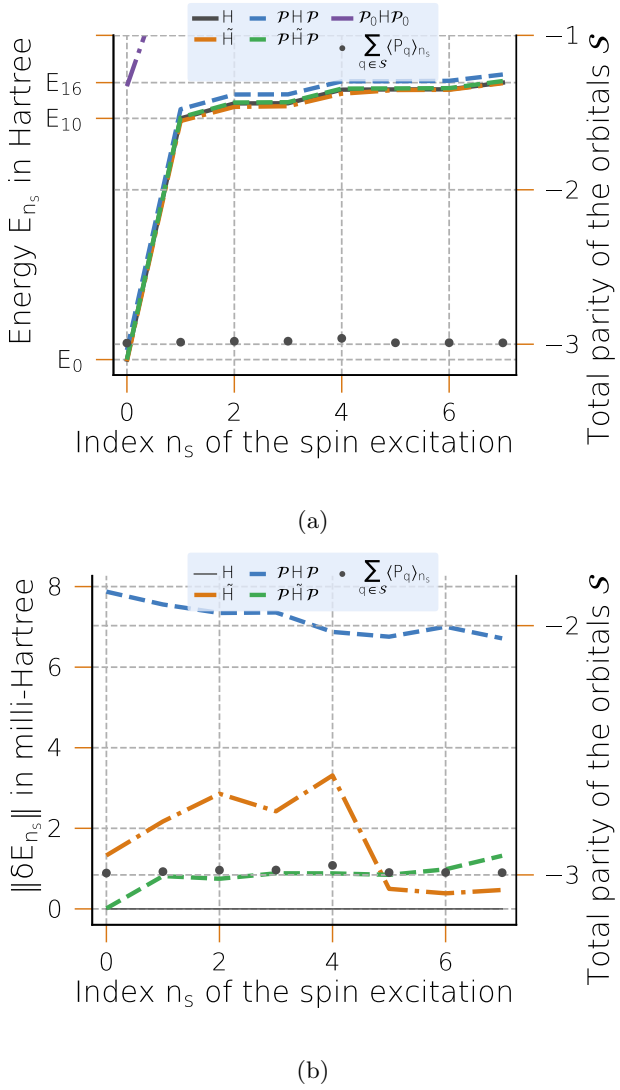


FIG. 9: (a) Low energy spectra of the respective Hamiltonians reduced to the set of eigenstates $|n_s\rangle$ of H and \tilde{H} , for which the expectation value of the total local parity for the spin-like orbitals ϕ_q satisfies $\sum_{q \in S} \langle P_q \rangle_{n_s} \simeq -3$. (b) Energy deviation $|\delta E_{n_s}|$ between the eigenenergies E_{n_s} of the full fermionic Hamiltonian and the respective transformed and projected, effective Hamiltonians. We observe that the spectrum of spinful excitations is better captured by the transformed Hamiltonians $\mathcal{P}\tilde{H}\mathcal{P}$ as opposed to the original Hamiltonian projected onto the subspace of the Hilbert space, where the spin-like orbitals become spin degrees of freedom, $\mathcal{P}HP$. The energy discrepancy between H and $\mathcal{P}\tilde{H}\mathcal{P}$ remains $|\delta E_{n_s}| \approx 1 \times 10^{-3}$ Hartree for the studied excited states. The corresponding discrepancy for the effective Hamiltonian $\mathcal{P}HP$ is noticeably larger and amounts to $|\delta E_{n_s}| \leq 8 \times 10^{-3}$ Hartree.

Hamiltonian \tilde{H} appears to remain a reasonable approximation to the original Hamiltonian H with $|\delta E_n| = |E_n^H - E_n^{\tilde{H}}| \leq 3 \times 10^{-3}$ Hartree. We find that the $n = 9$ lowest excited states correspond to an average local parity $\sum_{q \in S} \langle P_q \rangle_{n_s} \geq -1$. This implies the presence of either no spin degree freedom or at most one distinct local spin degree of freedom instead of a total of three distinct ones, such that the effective three-spin-system Hamiltonians $\mathcal{P}HP$ and $\mathcal{P}\tilde{H}\mathcal{P}$ are not sensible descriptions of the physics of the excited states with significant charge fluctuations. If we reduce the spectrum to eigenstates of H with three spin-like orbitals, i.e. total local parity $\sum_{q \in S} \langle P_q \rangle_{n_s} \simeq -3$, a different picture emerges. This reduced spectrum is shown in Fig. 9 (a). The corresponding energy discrepancies $|\delta E_{n_s}|$ from the true eigen energies of H are shown in Fig. 9 (b). The effective Hamiltonians $\mathcal{P}HP$ and $\mathcal{P}\tilde{H}\mathcal{P}$ appear to capture this reduced spectrum well. We observe a maximum energy discrepancy $|\delta E_{n_s}| = 1.5 \times 10^{-3}$ Hartree for the effective transformed Hamiltonian $\mathcal{P}\tilde{H}\mathcal{P}$, while we see a larger discrepancy $|\delta E_{n_s}| = 8 \times 10^{-3}$ Hartree for the effective Hamiltonian $\mathcal{P}HP$. The effective Hamiltonian \mathcal{P}_0HP_0 remains a bad approximation throughout this reduced energy spectrum. This highlights the necessity of a suitable orbital basis for the derivation of effective Hamiltonians describing the spin physics. In the parity-optimized orbital basis, for the given example of CrBr_6^{3-} , the terms coupling to the charge degree of freedom of the electron densities in the spin-like orbitals $\phi_{q \in S}$ are suppressed to the extent that the simple effective Hamiltonian $\mathcal{P}HP$ already becomes a relatively good description of the spin excitation spectrum. The subsequent Schrieffer-Wolff transformation and utilization of the corresponding effective transformed Hamiltonian $\mathcal{P}\tilde{H}\mathcal{P}$ then yield smaller additional improvements. This emphasizes the importance of using a suitable single particle basis. In contrast, we observe no such drastic suppression of the undesirable coupling terms for the basis of the CASSCF canonical molecular orbitals.

We have shown that our optimization procedure is able to correctly identify the $N_{\phi_q} = 3$ spin-like orbitals such that a subset of the energy spectrum of CrBr_6^{3-} can be accurately reproduced by a system of three spin degrees of freedom coupled to a fermionic environment. We further observe that our Schrieffer-Wolff transformation approach yields a transformed Hamiltonian \tilde{H} that, if projected to the Hilbert space representing three spins in a fermionic environment, improves upon the description given by the original Hamiltonian H projected to the same subspace. As shown in Fig. 9 the energy of the ground state and the low energy spin excited states are much closer to the original model if we apply our Schrieffer-Wolff method before projecting the spin-like orbitals on pure spin orbitals. We validate that the local parity of the spin-like basis orbitals can be regarded as a good indicator of the accuracy of the effective spin-bath Hamiltonian description $\mathcal{P}\tilde{H}\mathcal{P}$ derived with our method.

IV. CONCLUSION

Effective model Hamiltonians provide enormous value for the investigation of individual aspects of complex systems. Here, we have presented a procedure for the automatic derivation of model Hamiltonians of coupled spin degrees of freedom embedded in a fermionic environment. These Hamiltonians provide a means to enhance the study of the dominant low temperature spin physics of complex real materials. We have shown that to investigate the spin physics of such materials properly, one first needs to operate within a suitable single particle orbital basis, where a subset of the basis orbitals become realizations of spin degrees of freedom at low energies. We have introduced the local parity as a sensible metric for the spin-like behavior of electron densities in the basis orbitals. We have proven that the natural orbital basis does not generally correspond to the basis that features the spin-like orbitals. We have provided an example toy model for which the natural orbital basis is significantly worse than the initial basis for the study of spin physics. We also studied a well-known singlet-diradical molecule, namely closed configuration para-benzyne, and demonstrated that the two well-known non-trivial spin-like orbitals are correctly determined by our local parity optimization procedure. We find that the optimization of the local parity yields an orbital basis that typically results in a many particle basis of the Hilbert space with small coupling and significant energy gap between the different subspaces. Our extended Schrieffer-Wolff transformation method allows to also transform generic Hamiltonians with complicated interaction terms beyond the density-density interactions of the toy models that the Schrieffer-Wolff transformation has so far mostly been applied to. There is also no need for the block-diagonal part H_0 to be easily diagonalizable, because no calculation of the spectrum of H_0 is required in Schrieffer-Wolff transformation our method. We have shown that our Schrieffer-Wolff transformation method reproduces established results for the well-known single impurity Anderson model and the disordered Fermi-Hubbard model Hamiltonians. For these models we corroborate that the local parity of the spin-like orbitals is a good predictor for the quality of the effective spin-bath Hamiltonian as the description of the low energy spin dynamics. Lastly, we have applied the full spin-bath Hamiltonian derivation procedure to molecular chromium bromide. Here, we have shown that the derived effective spin-bath models are good descriptions of the system's low-energy spin excitations. We would like to point out that while we used an approximate multi reference method to determine the spin-like orbitals, the Schrieffer-Wolff mapping bypasses the standard quantum chemistry methods directly projecting the quantum chemistry model on the spin / spin-bath model. Being able to perform these calculations for quantum chemistry descriptions including all four index terms is provided by our representation of the Schrieffer-Wolff equation as a linear set of equations.

Future work will address more complex materials, where the Schrieffer-Wolff transformation becomes essential to obtain good effective Hamiltonian descriptions for the low-energy spin dynamics of the material.

DATA AVAILABILITY

The numerical data can be obtained from the authors on request. The spin finding procedure and the implemented Schrieffer Wolff transformation can be tested on <https://cloud.quantumsimulations.de/> using the HQS Spin Mapper module.

ACKNOWLEDGMENTS

We thank Reza Shirazi for insightful discussions. BMS, NE, and PS were supported by the Federal Ministry of Education and Research (BMBF) through the QSolid project (Grant no. 13N16155). BMS and PS acknowledge support by the BMBF through the MANIQU project (Grant no. 13N15576). VR was supported by the Federal Ministry for Economic Affairs and Climate Action through the AQUAS project (Grant no. 01MQ22003A).

Appendix A: Derivatives of the local parity

The analytic expression for the local parity $\langle P_q \rangle$ of the orbital ϕ_q after rotation as a function of the rotation angle θ and its derivatives are given by

$$\begin{aligned} \langle P_q \rangle = & -2 \left[\sum_{\sigma} \cos^2 \theta \langle c_{i\sigma}^{\dagger} c_{i\sigma} \rangle + \sin^2 \theta \langle c_{j\sigma}^{\dagger} c_{j\sigma} \rangle + \cos \theta \sin \theta (\langle c_{i\sigma}^{\dagger} c_{j\sigma} \rangle + \langle c_{j\sigma}^{\dagger} c_{i\sigma} \rangle) \right] \\ & + 4 \left[\cos^4 \theta \langle c_{i\uparrow}^{\dagger} c_{i\downarrow}^{\dagger} c_{i\downarrow} c_{i\uparrow} \rangle + \sin^4 \theta \langle c_{j\uparrow}^{\dagger} c_{j\downarrow}^{\dagger} c_{j\downarrow} c_{j\uparrow} \rangle \right. \\ & + \cos^3 \theta \sin \theta \left(\langle c_{i\uparrow}^{\dagger} c_{i\downarrow}^{\dagger} c_{i\downarrow} c_{j\uparrow} \rangle + \langle c_{i\uparrow}^{\dagger} c_{i\downarrow}^{\dagger} c_{j\downarrow} c_{i\uparrow} \rangle + \langle c_{i\uparrow}^{\dagger} c_{j\downarrow}^{\dagger} c_{i\downarrow} c_{i\uparrow} \rangle + \langle c_{j\uparrow}^{\dagger} c_{i\downarrow}^{\dagger} c_{i\downarrow} c_{i\uparrow} \rangle \right) \\ & + \cos \theta \sin^3 \theta \left(\langle c_{j\uparrow}^{\dagger} c_{j\downarrow}^{\dagger} c_{j\downarrow} c_{i\uparrow} \rangle + \langle c_{j\uparrow}^{\dagger} c_{j\downarrow}^{\dagger} c_{i\downarrow} c_{j\uparrow} \rangle + \langle c_{j\uparrow}^{\dagger} c_{i\downarrow}^{\dagger} c_{j\downarrow} c_{j\uparrow} \rangle + \langle c_{i\uparrow}^{\dagger} c_{j\downarrow}^{\dagger} c_{j\downarrow} c_{j\uparrow} \rangle \right) \\ & + \cos^2 \theta \sin^2 \theta \left(\langle c_{i\uparrow}^{\dagger} c_{i\downarrow}^{\dagger} c_{j\downarrow} c_{j\uparrow} \rangle + \langle c_{i\uparrow}^{\dagger} c_{j\downarrow}^{\dagger} c_{j\downarrow} c_{i\uparrow} \rangle + \langle c_{j\uparrow}^{\dagger} c_{j\downarrow}^{\dagger} c_{i\downarrow} c_{i\uparrow} \rangle + \langle c_{j\uparrow}^{\dagger} c_{i\downarrow}^{\dagger} c_{i\downarrow} c_{j\uparrow} \rangle \right. \\ & \left. + \langle c_{j\uparrow}^{\dagger} c_{i\downarrow}^{\dagger} c_{j\downarrow} c_{i\uparrow} \rangle + \langle c_{i\uparrow}^{\dagger} c_{j\downarrow}^{\dagger} c_{i\downarrow} c_{j\uparrow} \rangle \right) \Big] + 1, \end{aligned} \quad (A1)$$

$$\begin{aligned} \frac{d\langle P_q \rangle}{d\theta} = & 4 \sin \theta \cos \theta \left(\sum_{\sigma} \langle c_{i\sigma}^{\dagger} c_{i\sigma} \rangle - \langle c_{j\sigma}^{\dagger} c_{j\sigma} \rangle \right) + 2(\sin^2 \theta - \cos^2 \theta) \left(\sum_{\sigma} \langle c_{i\sigma}^{\dagger} c_{j\sigma} \rangle + \langle c_{j\sigma}^{\dagger} c_{i\sigma} \rangle \right) \\ & + 4 \left[(-4) \sin \theta \cos^3 \theta \langle c_{i\uparrow}^{\dagger} c_{i\downarrow}^{\dagger} c_{i\downarrow} c_{i\uparrow} \rangle + 4 \sin^3 \theta \cos \theta \langle c_{j\uparrow}^{\dagger} c_{j\downarrow}^{\dagger} c_{j\downarrow} c_{j\uparrow} \rangle \right. \\ & + 2 (\sin \theta \cos^3 \theta - \sin^3 \theta \cos \theta) \langle A \rangle \\ & + (-\sin^4 \theta + 3 \sin^2 \theta \cos^2 \theta) \langle B \rangle \\ & \left. + (\cos^4 \theta - 3 \sin^2 \theta \cos^2 \theta) \langle C \rangle \right], \end{aligned} \quad (A2)$$

$$\begin{aligned} \frac{d^2\langle P_q \rangle}{d\theta^2} = & \left[\sum_{\sigma} 4 (\cos^2 \theta - \sin^2 \theta) (\langle c_{i\sigma}^{\dagger} c_{i\sigma} \rangle - \langle c_{j\sigma}^{\dagger} c_{j\sigma} \rangle) + 8 \sin \theta \cos \theta (\langle c_{i\sigma}^{\dagger} c_{j\sigma} \rangle + \langle c_{j\sigma}^{\dagger} c_{i\sigma} \rangle) \right] \\ & + 4 \left[(-4 \cos^4 \theta + 12 \sin^2 \theta \cos^2 \theta) \langle c_{i\uparrow}^{\dagger} c_{i\downarrow}^{\dagger} c_{i\downarrow} c_{i\uparrow} \rangle \right. \\ & + (-4 \sin^4 \theta + 12 \sin^2 \theta \cos^2 \theta) \langle c_{j\uparrow}^{\dagger} c_{j\downarrow}^{\dagger} c_{j\downarrow} c_{j\uparrow} \rangle \\ & + (2 \sin^4 \theta + 2 \cos^4 \theta - 12 \sin^2 \theta \cos^2 \theta) \langle A \rangle \\ & + (6 \sin \theta \cos^3 \theta - 10 \sin^3 \theta \cos \theta) \langle B \rangle \\ & \left. + (-10 \sin \theta \cos^3 \theta + 6 \sin^3 \theta \cos \theta) \langle C \rangle \right], \end{aligned} \quad (A3)$$

where we have abbreviated

$$\begin{aligned}
\langle A \rangle &= \left(\langle c_{i\uparrow}^\dagger c_{i\downarrow}^\dagger c_{j\downarrow} c_{j\uparrow} \rangle + \langle c_{i\uparrow}^\dagger c_{j\downarrow}^\dagger c_{j\downarrow} c_{i\uparrow} \rangle + \langle c_{j\uparrow}^\dagger c_{j\downarrow}^\dagger c_{i\downarrow} c_{i\uparrow} \rangle \right. \\
&\quad \left. + \langle c_{j\uparrow}^\dagger c_{i\downarrow}^\dagger c_{i\downarrow} c_{j\uparrow} \rangle + \langle c_{j\uparrow}^\dagger c_{i\downarrow}^\dagger c_{j\downarrow} c_{i\uparrow} \rangle + \langle c_{i\uparrow}^\dagger c_{j\downarrow}^\dagger c_{i\downarrow} c_{j\uparrow} \rangle \right), \\
\langle B \rangle &= \left(\langle c_{j\uparrow}^\dagger c_{j\downarrow}^\dagger c_{j\downarrow} c_{i\uparrow} \rangle + \langle c_{j\uparrow}^\dagger c_{j\downarrow}^\dagger c_{i\downarrow} c_{j\uparrow} \rangle + \langle c_{j\uparrow}^\dagger c_{i\downarrow}^\dagger c_{j\downarrow} c_{j\uparrow} \rangle + \langle c_{i\uparrow}^\dagger c_{j\downarrow}^\dagger c_{j\downarrow} c_{j\uparrow} \rangle \right), \\
\langle C \rangle &= \left(\langle c_{i\uparrow}^\dagger c_{i\downarrow}^\dagger c_{i\downarrow} c_{j\uparrow} \rangle + \langle c_{i\uparrow}^\dagger c_{i\downarrow}^\dagger c_{j\downarrow} c_{i\uparrow} \rangle + \langle c_{i\uparrow}^\dagger c_{j\downarrow}^\dagger c_{i\downarrow} c_{i\uparrow} \rangle + \langle c_{j\uparrow}^\dagger c_{i\downarrow}^\dagger c_{i\downarrow} c_{i\uparrow} \rangle \right).
\end{aligned}$$

Appendix B: Symmetry-specification of fermionic creation and annihilation operators

We demonstrate the concept of symmetry-specified block-offdiagonal operators for the case of fermionic creation and annihilation operators. For a single orbital the local Hilbert space is given by

$$\mathcal{H}_{\text{local}} = \{|0\rangle, |\uparrow\rangle, |\downarrow\rangle, |\uparrow\downarrow\rangle\}, \quad (\text{B1})$$

where we have fixed the order \uparrow, \downarrow for the fermionic sign. The fermionic annihilation operator $c_\downarrow : \mathcal{H}_{\text{local}} \rightarrow \mathcal{H}_{\text{local}}$ for fermions with spin $s_z = -\frac{1}{2}$ acts on the vectors in the local Hilbert space and performs the linear map

$$\begin{aligned}
c_\downarrow(a_0|0\rangle + a_\uparrow|\uparrow\rangle + a_\downarrow|\downarrow\rangle + a_{\uparrow\downarrow}|\uparrow\downarrow\rangle) \\
= a_0\mathbf{0}_{\mathcal{H}} + a_\uparrow\mathbf{0}_{\mathcal{H}} + a_\downarrow|0\rangle + (-a_{\uparrow\downarrow})|\uparrow\rangle,
\end{aligned} \quad (\text{B2})$$

where $\mathbf{0}_{\mathcal{H}}$ denotes the zero element of the Hilbert space. We see that c_\downarrow maps two of the states, namely $|0\rangle$ and $|\uparrow\rangle$, map to the zero element. There are thus two non-vanishing components of c_\downarrow which map $|\downarrow\rangle \rightarrow |0\rangle$ and $|\uparrow\downarrow\rangle \rightarrow |\uparrow\rangle$. We can choose to distinguish the blocks of the Hilbert space based on their total particle number $n = \sum_\sigma c_\sigma^\dagger c_\sigma$. We consequently identify the state $|\uparrow\downarrow\rangle$ as belonging to the block characterized by the eigenvalue $\Lambda_q = n = 2$ and state $|\downarrow\rangle$ to the block characterized by the eigenvalue $\Lambda_q = n = 1$. Given the choice of n as the operator distinguishing the blocks of the Hilbert space, an intuitive choice for the operator A is the local number of fermions with opposite spin $s_z = \frac{1}{2}$, i.e. the operator $n_\uparrow = c_{\uparrow}^\dagger c_{\uparrow}$. It is easily seen that the choice $A = n_\uparrow$ satisfies

$$[n, n_\uparrow] = 0, \quad (\text{B3})$$

$$[c_\downarrow, n_\uparrow] = 0, \quad (\text{B4})$$

where eq. (B3) highlights that n_\uparrow commutes with all operators that are block-diagonal in our choice of blocks distinguish by n . The operator n_\uparrow has eigenvalues $\lambda_q \in \{0, 1\}$. Using equations (22) and (24) we can express the operator c_\downarrow as sum of unique components

$$\begin{aligned}
c_\downarrow &= \alpha_0 (n_\uparrow - 1) c_\downarrow + \alpha_1 (n_\uparrow - 0) c_\downarrow \\
&= -(n_\uparrow - 1) c_\downarrow + (n_\uparrow - 0) c_\downarrow \\
&= (1 - n_\uparrow) c_\downarrow + n_\uparrow c_\downarrow \\
&= c_{\lambda_q=0,\downarrow} + c_{\lambda_q=1,\downarrow}.
\end{aligned} \quad (\text{B5})$$

The separation of c_\downarrow into its unique components can also be achieved by multiplying it with the identity $\mathbf{1} = (1 - n_\uparrow) + n_\uparrow$. We expand the Hermitian conjugate operator c_\downarrow^\dagger in the same way as

$$c_\downarrow^\dagger = c_{\lambda_q=0,\downarrow}^\dagger + c_{\lambda_q=1,\downarrow}^\dagger = (1 - n_\uparrow) c_\downarrow^\dagger + n_\uparrow c_\downarrow^\dagger, \quad (\text{B6})$$

and find

$$\begin{aligned}
[c_{\lambda_q=0,\downarrow}, c_{\lambda_q=0,\downarrow}^\dagger] &= (1 - n_\uparrow) (1 - n_\uparrow) [c_\downarrow, c_\downarrow^\dagger] \\
&= (1 - n_\uparrow) (1 - 2c_\downarrow^\dagger c_\downarrow) \\
[c_{\lambda_q=0,\downarrow}, c_{\lambda_q=1,\downarrow}^\dagger] &= (1 - n_\uparrow) n_\uparrow [c_\downarrow, c_\downarrow^\dagger] = 0 \\
[c_{\lambda_q=1,\downarrow}, c_{\lambda_q=0,\downarrow}^\dagger] &= n_\uparrow (1 - n_\uparrow) [c_\downarrow, c_\downarrow^\dagger] = 0 \\
[c_{\lambda_q=1,\downarrow}, c_{\lambda_q=1,\downarrow}^\dagger] &= n_\uparrow n_\uparrow [c_\downarrow, c_\downarrow^\dagger] = n_\uparrow (1 - 2c_\downarrow^\dagger c_\downarrow).
\end{aligned} \quad (\text{B7})$$

- [1] W. Heisenberg, *Zeitschrift für Physik* **49**, 619–636 (1928).
- [2] H. Günther, *NMR Spectroscopy: Basic Principles, Concepts and Applications in Chemistry* (John Wiley & Sons, 2013).
- [3] V. Veryazov, P. Å. Malmqvist, and B. O. Roos, *International Journal of Quantum Chemistry* **111**, 3329–3338 (2011), <https://onlinelibrary.wiley.com/doi/10.1002/qua.23068>.
- [4] S. McArdle, S. Endo, A. Aspuru-Guzik, S. Benjamin, and X. Yuan, arXiv:1808.10402 [quant-ph] (2018), arXiv: 1808.10402.
- [5] W. Pouse, L. Peeters, C. Hsueh, U. Gennser, A. Cavanna, M. A. Kastner, A. K. Mitchell, and D. Goldhaber-Gordon, *Nat. Phys.*, 492–499 (2023).
- [6] R. G. Shirazi, B. M. Schoenauer, P. Schmitteckert, M. Marthaler, and V. Rybkin, “Understanding rad-

icals via orbital parities,” (2024), arXiv:2404.18787 [physics.chem-ph].

[7] J. Schrieffer and P. Wolff, *Physical Review* **149**, 491 (1966).

[8] L. L. Foldy and S. A. Wouthuysen, *Physical Review* **78**, 29 (1950), publisher: American Physical Society.

[9] S. Bravyi, D. DiVincenzo, and D. Loss, *Annals of Physics* **326**, 2793 (2011), arXiv: 1105.0675.

[10] G. T. Landi, “Eigenoperator approach to Schrieffer-Wolff perturbation theory and dispersive interactions,” (2024), arXiv:2409.10656 [cond-mat, physics:hep-th, physics:quant-ph].

[11] J. Wurtz, P. Claeys, and A. Polkovnikov, arXiv:1910.11889 [cond-mat] (2019), 10.1103/PhysRevB.101.014302, arXiv: 1910.11889.

[12] F. Wegner, *Annalen der Physik* **506**, 77 (1994).

[13] H. Krull, N. A. Drescher, and G. S. Uhrig, *Physical Review B* **86**, 125113 (2012), publisher: American Physical Society.

[14] G. Schmiedinghoff and G. S. Uhrig, *SciPost Physics* **13**, 122 (2022).

[15] S. R. White, *The Journal of Chemical Physics* **117**, 7472 (2002), https://pubs.aip.org/aip/jcp/article-pdf/117/16/7472/19317208/7472_1_online.pdf.

[16] A. H. MacDonald, S. M. Girvin, and D. Yoshioka, *Physical Review B* **37**, 9753 (1988), publisher: American Physical Society.

[17] V. I. Anisimov, J. Zaanen, and O. K. Andersen, *Phys. Rev. B* **44**, 943 (1991).

[18] E. Macke, I. Timrov, N. Marzari, and L. C. Ciacchi, *Journal of Chemical Theory and Computation* **20**, 4824–4843 (2024), pMID: 38820347, <https://doi.org/10.1021/acs.jctc.3c01403>.

[19] A. Georges, G. Kotliar, W. Krauth, and M. J. Rozenberg, *Rev. Mod. Phys.* **68**, 13 (1996).

[20] G. Kotliar, S. Y. Savrasov, K. Haule, V. S. Oudovenko, O. Parcollet, and C. A. Marianetti, *Rev. Mod. Phys.* **78**, 865 (2006).

[21] D. Vollhardt, “Dynamical mean-field theory of strongly correlated electron systems,” in *Proceedings of the International Conference on Strongly Correlated Electron Systems (SCES2019)* (2019) <https://journals.jps.jp/doi/pdf/10.7566/JPSCP.30.011001>.

[22] F. Aryasetiawan, K. Karlsson, O. Jepsen, and U. Schonberger, *Physical Review B* **74**, 125106 (2006), arXiv: cond-mat/0603138.

[23] M. Springer and F. Aryasetiawan, *Phys. Rev. B* **57**, 4364 (1998).

[24] F. Aryasetiawan, M. Imada, A. Georges, G. Kotliar, S. Biermann, and A. I. Lichtenstein, *Phys. Rev. B* **70**, 195104 (2004).

[25] K. Karlsson, F. Aryasetiawan, and O. Jepsen, *Phys. Rev. B* **81**, 245113 (2010).

[26] C. Honerkamp, H. Shinaoka, F. F. Assaad, and P. Werner, *Phys. Rev. B* **98**, 235151 (2018).

[27] G. H. Wannier, *Phys. Rev.* **52**, 191 (1937).

[28] W. Kohn, *Phys. Rev.* **115**, 809 (1959).

[29] N. Marzari, A. A. Mostofi, J. R. Yates, I. Souza, and D. Vanderbilt, *Rev. Mod. Phys.* **84**, 1419 (2012).

[30] A. Liechtenstein, M. Katsnelson, V. Antropov, and V. Gubanov, *Journal of Magnetism and Magnetic Materials* **67**, 65–74 (1987).

[31] X. He, N. Helbig, M. J. Verstraete, and E. Bousquet, *Computer Physics Communications* **264**, 107938 (2021).

[32] R. Penrose, *Mathematical Proceedings of the Cambridge Philosophical Society* **52**, 17 (1956).

[33] T. Helgaker, P. Jorgensen, and J. Olsen, *Molecular Electronic-Structure Theory* (John Wiley & Sons, Ltd, 2000) pp. 523–597.

[34] P.-O. Löwdin, *Physical Review* **97**, 1474 (1955), publisher: American Physical Society.

[35] R. Lindh and B. J. Persson, *Journal of the American Chemical Society* **116**, 4963 (1994).

[36] L. Salem and C. Rowland, *Angewandte Chemie International Edition in English* **11**, 92 (1972).

[37] R. McWeeny and C. A. Coulson, *Proceedings of the Royal Society of London. Series A. Mathematical and Physical Sciences* **241**, 239 (1977), publisher: Royal Society.

[38] B. O. Roos, P. R. Taylor, and P. E. Sigbahn, *Chemical Physics* **48**, 157–173 (1980).

[39] K. P. Lawley, *Ab Initio Methods in Quantum Chemistry, Volume 69, Part 2* (John Wiley & Sons, 2009).

[40] P. W. Anderson, *Physical Review* **124**, 41 (1961), publisher: American Physical Society.

[41] S. K. Kehrein and A. Mielke, *Annals of Physics* **252**, 1 (1996).

[42] R. U. Haq and K. Singh, arXiv:2004.06534 [cond-mat] (2020), arXiv: 2004.06534.

[43] A. C. Hewson, *The Kondo Problem to Heavy Fermions* (Cambridge University Press, 1997).

[44] J. Hubbard, *Proceedings of the Royal Society of London. Series A. Mathematical and Physical Sciences* , 238 (1963).

[45] F. H. L. Essler, H. Frahm, F. Göhmann, A. Klümper, and V. E. Korepin, *The One-Dimensional Hubbard Model* (Cambridge University Press, 2005).

[46] C. Gong, L. Li, Z. Li, H. Ji, A. Stern, Y. Xia, T. Cao, W. Bao, C. Wang, Y. Wang, Z. Q. Qiu, R. J. Cava, S. G. Louie, J. Xia, and X. Zhang, *Nature* **546**, 265 (2017).

[47] B. Huang, G. Clark, E. Navarro-Moratalla, D. R. Klein, R. Cheng, K. L. Seyler, D. Zhong, E. Schmidgall, M. A. McGuire, D. H. Cobden, W. Yao, D. Xiao, P. Jarillo-Herrero, and X. Xu, *Nature* **546**, 270 (2017).

[48] D. L. Esteras and J. J. Baldoví, *Materials Today Electronics* **6**, 100072 (2023).

[49] HQS Quantumsimulations GmbH, “ActiveSpaceFinder,” (2024), github.com/HQSquantumsimulations/ActiveSpaceFinder.